Evolutionary Systematics. 8 2024, 65–90 | DOI 10.3897/evolsyst.8.117735

PENSOFT

EVOLUTIONARY SYSTEMATICS

Application of extended depth of field 3D imagery to tackle the challenges of cryptic species: a use case in the genus *Betiscoides* Sjöstedt, 1924 (Orthoptera, Caelifera, Lentulidae) and its taxonomic implications

Daniela Matenaar[1]

1 *Hessisches Landesmuseum Darmstadt (HLMD), Friedensplatz 1, 64283 Darmstadt, Germany*

https://zoobank.org/6B534FD5-542C-4636-87D1-1738CE33D9F8

Corresponding author: Daniela Matenaar (daniela.matenaar@gmail.com)

Academic editor: Martin Husemann ♦ **Received** 22 December 2023 ♦ **Accepted** 6 March 2024 ♦ **Published** 25 March 2024

Abstract

Discovering and handling cryptic diversity among species challenges taxonomists around the world. This is particularly true for the most diverse animal class – the insects – with cryptic diversity, apart from vast species numbers, being one of the main factors that hamper the description of new species. The biodiversity hotspot Cape Floristic Region of South Africa harbors many endemic and yet undescribed insect species, inter alia, Orthoptera. In this study, extended depth of field and 3D imagery enabled for a novel assessment of the external morphological characteristics used for defining and describing the genetically highly diverse genus *Betiscoides* Sjösdtedt, 1924, leading to a new definition of the genus' characteristics as well as a revision of character traits of the known species. Two new species are described and a key to all five recognized *Betiscoides* species is provided. Application standards are derived to enable replicable and reliable image acquisition and measuring. These findings shall contribute to promote efforts being made to establish image based taxonomic identification for researchers worldwide. High-resolution images provide the basis to train deep learning algorithms/ tools, to detect the smallest differences in highly morphologically alike species, and to implement this knowledge in global species monitoring and conservation action to prevent further species loss.

Key Words

Image based taxonomy, molecular genetics, divergent evolutionary lineage, deep learning, photogrammetry

Introduction

Perhaps it is in the nature of things that with an estimate of around 10 million species (Mora et al. 2011; Larsen et al. 2017; Stork 2018) and comparatively few taxonomist experts (European Commission 2022), we are still far from identifying and adequately describing the majority of species on Earth. Limited accessibility either in situ (habitat) or ex situ (museum collections) and difficult detectability (small size <1 mm) of species, are also responsible for the "taxonomic deficit" and cause a respective shift towards invertebrates and microbes (Blaxter et al. 2005). Amidst the overwhelming crisis of biodiversity loss, identification of species based on their external morphological characteristics remains one of the fundamental tools in nature conservation since it enables different kind of stakeholders to identify the species in the field and/ or to derive certain conservation measures. In recent years, improvements have been achieved on many levels. For instance, photogrammetric methods for small species have been developed and improved lately (Ströbel et al. 2018), making the morphological analyses more precise, replicable and timesaving in the end. Aside from that, in order to accomplish the detection of species and their distribution ranges extensively, scientists depend on the help of amateurs and citizen partic-

ipation. This support is nowadays greater than ever and becomes apparent through reports in online portals such as https://www.inaturalist.org/ or https://observation.org/ etc. These portals are widely used and a powerful, helpful measure also resulting in the discovery of new species and serving as a monitoring tool and availing in the assessment of global biodiversity.

However, up to date one issue remains unsolved: the integration of cryptic diversity (in image based deep learning algorithms), as discrimination among cryptic species challenges taxonomists around the world (Li and Wiens 2023). The problem is prevailing and it was even proposed to refrain from traditional species concepts but to stick to OTUs instead (Green et al. 2004; Blaxter et al. 2005; Rosselló-Mora and López-López 2014). However, delimitation and diversity detection remains limited as OTUs, divergent evolutionary lineages (DELs) or "Barcode-Index-Numbers" (BINs – (referenced in the Barcode of Life Data System; Hawlitschek et al. 2017; Høye et al. 2021) are also not always clear to derive and not equally reliable among different groups of taxa. For instance, using COI as barcoding gene turned out to be erroneous in Caelifera (Orthoptera) due to various reasons (Hawlitschek et al. 2017). In general, cryptic diversity torpedoes any attempt to estimate actual species diversity in the end. However, it is more important than ever to identify and describe species and their diversity to initiate protection measures before habitat destruction will result in its ultimate loss.

Up to date, the drivers of cryptic diversity are not fully understood and consequently the global distribution of cryptic diversity remains unclear. For instance, it is not proven, that cryptic diversity is greater in tropical than in temperate regions (Poulin and Pérez-Ponce de León 2017). However, there is a tendency towards a correlation of diverse habitat structure and high rates of diversification with increased occurrence of cryptic diversity. South Africa houses one of the earths' six floral kingdoms and is known for its tremendous biodiversity, including high numbers of endemic species and a high level of cryptic diversity, especially in invertebrates (Tolley et al. 2014). The genus *Betiscoides* belongs to the wingless Orthoptera family Lentulidae, with Southern Africa as the main area of its distribution. Taxonomy within this family, especially in Southern African taxa is incomplete and inaccurate and is likely to contain a high level of cryptic diversity (Cigliano et al. 2023). Recently, new species within the Lentulidae were described and certain genera revised (Otte 2014a, 2014b, 2015, 2020; Otte et al. 2023). *Betiscoides* is endemic to the Cape Floristic Region, South Africa and all known species are considered "endangered" (Hochkirch 2012a, 2012b, 2012c). The three recognized nominal species in *Betiscoides* are *Betiscoides meridionalis* Sjöstedt, 1924, *Betiscoides parva* Key, 1937 and *Betiscoides sjostedti* Key, 1937. Key (1937) recognized early on the challenges regarding the clarification of the taxonomy of *Betiscoides*, stating in his manuscript "the genus has every appearance of being a difficult one". Molecular genetic analyses of *Betiscoides* revealed high genetic diversity and resulted in 24 divergent evolutionary lineages (Matenaar et al. 2018). A first and brief morphological assessment of the DELs showed high intraspecific variability making delimitation difficult and the presence of a cryptic species complex likely (Matenaar et al. 2018).

In this study, I aim at finding and defining fine scale morphological characteristics and diagnostic characters suitable for distinguishing the DELs of *Betiscoides* by applying 3D and extended depth of field (EDOF) image based analysis. These findings shall contribute to identify external morphological structures relevant for taxonomic differentiation in invertebrates and, in general, to derive application standards (best practice) to support the development of deep learning algorithms suitable for rare and cryptic species.

Materials and methods

Fieldwork and taxon sampling

Specimens were collected by hand and via sweep netting in the years 2011–2013, 2016 and 2020 (permit numbers AAA007-00374-0035 (28/11/2011), AAA007-00197-0056 (15/03/ 2016, CN44-59-11619 (11/11/2019)) on Jonaskop and on the plateau of Groot Winterhoek Wilderness Area, South Africa (Fig. 1). Collected specimens were killed in a freezer. Afterwards they were dried and pinned. Prior to that, one hind leg was detached from the body before drying and kept frozen for subsequent DNA extraction. In order to reconstruct phylogenies and determine species affiliation (of the voucher specimens), the taxon set published in Matenaar et al. (2018) was used and extended by sequences of the voucher specimens. The description of the species novae are based on molecular and morphological data. Specimens were deposited in the invertebrate collection of Hessisches Landesmuseum Darmstadt (HLMD).

Molecular analyses

DNA extraction of specimens HLMD-Cael-4HT, B168; HLMD-Cael-18AT, B166; HLMD-Cael-8PT, B162; HLMD-Cael-10PT, B163; HLMD-Cael-14PT, B165; HLMD-Cael-15PT, B167; HLMD-Cael-364HT, B156; HLMD-Cael-368AT, B155; HLMD-Cael-362PT, B153; HLMD-Cael-367PT, B154, HLMD-Cael-379PT, B169 was conducted in March 2022 using the Quiagen DNAEasy Blood and Tissue Kit. DNA was isolated from the specimens' hind leg muscle. Further processing (PCR, purification and sequencing) of gDNA took place at Macrogen, Netherlands. Three mitochondrial genes were sequenced: 12S rRNA, NDS (16S rRNA, t-LEU and NADH-Dehydrogenase subunit1), ND5 (NADH-Dehydrogenase subunit 5). Numbers added to the museum collection numbers starting with B, e.g. B168, are running, internally used, numbers of *Betiscoides* specimens, for further information see Suppl. material 1.

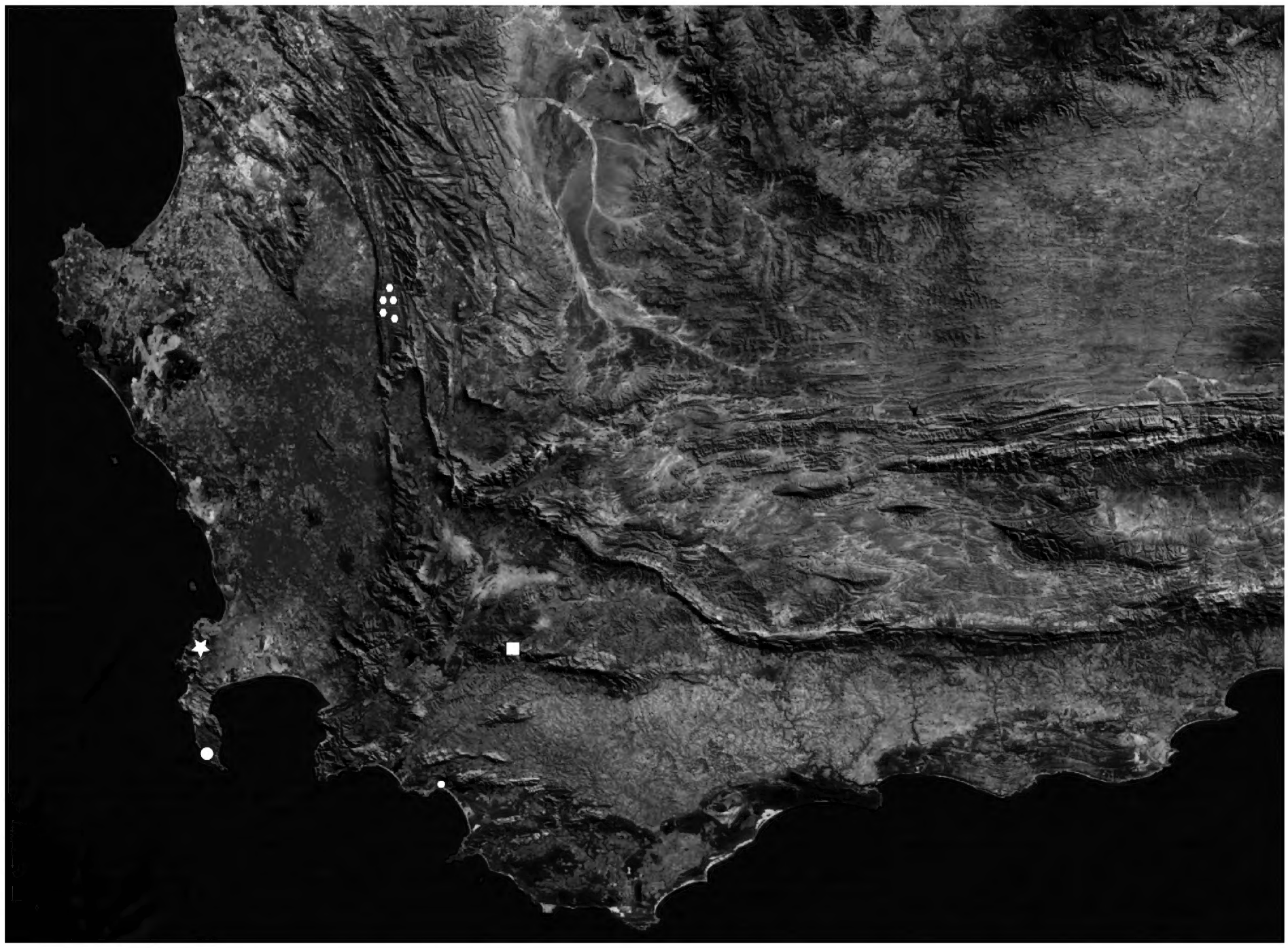

Figure 1. Map of the southwestern area of South Africa including the type localities of the *Betiscoides* species. Star = Table Mountain, type locality of *Betiscoides sjostedti* Key, 1937. Circle = type locality of *B. parva* Key, 1937 and the collection site of *B. meridionalis* specimens, Key (1937) used for the revised description of the species. One paratype of *B. parva* was collected in Hermanus, which is indicated by the smaller circle. Square = Jonaskop, type locality of *B. nova* sp. nov., hexagon = Groot Winterhoek, type localities of *B. muris* sp. nov. All type localities are situated in the Western Cape province of South Africa. @ Source satellite image by Bing, downloaded on 24 November 2023.

Sequence analysis

Sequences were inspected and aligned using MEGA X (Kumar et al. 2018) and added to the taxon set of Matenaar et al. (2018). Furthermore, the sequences of *Betiscoides* from the taxon set of Matenaar et al. (2016; specimen numbers: "*Betiscoides* 9–12, 19–24, 26, 28") were added. Sample denotations were adjusted to the sample denotations used in Matenaar et al. (2018), "L" was added to the denotation to avoid overlapping, e.g. "*Betiscoides* 9" is "LB_9", and to maintain the reference to the phylogenetic reconstruction in Matenaar et al. (2016). Sample denotations in the phylogenetic tree consist of the specimen number, abbreviation of the collection locality and plot number (e.g. B6_jo_07). The starting position was detected by eye. ClustalW was applied to align sequences. The gap opening penalty was set to 15 for pairwise and multiple alignments and the gap extension penalty was set to 6.66. IUB was chosen as DNA Weight Matrix with a transition weight of 0.5. Delay Divergent cut-off was set to 30%. Genetic distances between the clades were calculated using p-distance setting in MEGA. The division in divergent evolutionary units was applied accordingly to Matenaar et al. (2018). Original names were only used for specimens collected at, or very close to, their type localities and matching the morphology of the type material. Prior to tree reconstruction with Bayesian inference, partitions and the best-suited substitution model applicable in MrBayes were detected using Partitionfinder (Lanfear et al. 2012). Subsets were determined before Partitionfinder was run by dividing NDS in the components 16S (including t-Leu) and ND1 as well as the coding genes into their coding positions. In total, six different partitions with different substitution models were calculated. The model HYK+I+G was chosen for 12S, 16S and first coding position of ND1 and ND5; GTR+I+G was used for both partitions consisting of the second coding positions of ND1 and ND5 respectively as well as for the first and second coding positions of H3. The third coding positions of ND1 and ND5 were grouped as one partition with the model HKY+G. The model F81+G was chosen for ITS2 and SYM+I+G for the third coding position of H3. I performed the Bayesian analysis using MrBayes v.3.1.2 (Huelsenbeck and Ronquist 2001; Ronquist and

Huelsenbeck 2003). The analysis was run for 10 million generations, sampling trees every 1,000 generations. The first 2,500 trees were discarded before a consensus tree was calculated and visualized in FIGTREE v. 1.3.1 (Rambaut 2016). Maximum likelihood reconstruction was performed in RAxMLGUI1.5b1 (Silvestro and Michalak 2012) using the ML+thorough bootstrap method with 500 replicates. The GTR+I+G model was chosen for the complete data set.

Morphological analysis

External morphological characters were analyzed and measured using Leica M165 C and Keyence VHX 7000 microscope. Morphometrics (in millimetres) taken with Leica M165 C were measured with a measuring eyepiece. Pictures were taken with Keyence VHX 7000 microscope. Plane 2D and 3D Volume measurements were digitally conducted using the Keyence VHX 7000 microscope and its integrated software. Settings were adapted to the specific requirements and are detailed in figure legends. Profile analysis in 3D (eyes, prosternal process, female ovipositor valves) was conducted on 100 or 150× HDR images of the end of the abdomen. Sufficient quality of the images was checked prior the analysis by assessing the "point height". I attempted to achieve an automated counting of hairy structures on the deep focus images and used the automated counting of extracted shapes tool integrated in the Keyence VHX 7000 software. In order to accomplish that, I took an ×150 3D depth composition image in HDR mode. Hereby, I stopped the image stacking when the area had been fully captured, which I wanted to analyze. This procedure should ensure that interferences were prevented. Then, I used the "auto area measurement" function, the extraction method was set to "Brightness" 113 to 255, and shaping was done by eliminating grains in the size of an area of > 1 mm^2. In the last step, "Inversion" was used to achieve that the end of the abdomen was extracted except for the hairy structures framing it. Eye volume measurement was done by manually specifying the Z-axis according to the visible base of the eye. A polygon was drawn along the visible callus line framing the eyes and the volume was automatically calculated. 3D Images and outputs of the profile and volume measurements are exemplarily shown in Fig. 2. In order to generate the body volume, specimens were scanned using the DISC3D Scanner and the DISC3D Control Software. In total, 398 extended depth of field (EDOF) images of each specimen were taken and imported as "single cameras" into Metashape Pro. Settings for the import were: accuracy "highest", generic, reference preselection "yes", key, and tie point limit "250000", exclude stationary points "yes" guided image matching "no". In order to optimize the cameras "check f only" was chosen. Parameters to build the mesh were set as follows: Source "depth maps", surface type "Arbitrary 3D", quality "ultra high", face count "high", advanced: interpolation "enabled (default)", depth filtering "mild", calculate vertex colors "yes". The needle was removed by choosing the free form selection tool and close holes was set to 100%. Texture was built by setting texture type to "Diffuse Map", source data "Images", Mapping mode "Generic", blending mode "mosaic (default)", texture size/count "5000, 1", advanced "enable hole filling "yes", enable ghosting filter "yes". Body volume was measured by calculating the volume and area of the mesh automatically. Female body volumes were not calculated due to the natural physical changes of the female body during life span (before or after laying eggs, while carrying eggs).

Terminology

Terminology applied for morphological characters is based on Dirsh (1965) and in specific parts on Key (1937). However, alterations are made when describing the prosternal process. Key (1937) used a terminus (laminate) which is not clear and although Dirsh (1965) defined 13 different shapes of prosternal processes, he did not apply any of these on *Betiscoides*. Thus, I refrain from using Keys and Dirshs terms regarding the prosternal process and implement the following terms for descriptions: T-shape, thin lamelliform, thick lamelliform, and trapezoid. BL refers to the length of the body, head length (HL) refers to the dorsal distance from the tip of the fastigium to the beginning of the pronotum, diagonal head length (HDL) refers to the distance from the tip of the fastigium to lower end of the head, in profile, head height (HH) refers to the distance from the dorsal to the ventral part of the head, in profile. PL means pronotum length and HFL stands for hind femoral length. Degree of male subgenital plate refers to the angular degree of the tip of the subgenital plate in males, measured in lateral view along the upper and lower side of the subgenital plate. In addition, I hereby introduce the following characters summarized as "females genital characters", which include the following: upper valve degree = angular degree of the tip of the dorsal valve, upper valve distance = length from fold to tip of dorsal valve, upper valve width = width at the fold of dorsal valve, Pr = Protrusion = preapical part of the ventral valve, protrusion degree = angular degree of protrusion measured along protrusion line 1 and 2, protrusion line 1 = anterior line of protrusion, protrusion line 2 = posterior line of protrusion, protrusion distance = the distance between the start of protrusion line 1 and 2, protrusion vertical distance = vertical distance between the lowest tip of protrusion to the tip of the ventral valve (see Fig. 3). The 3D measurements of the eye are described by longitudinal height = the distance between the lowest to the highest elevation of the eye measured in longitudinal direction, cross-sectional height = the distance between the lowest to the highest elevation of the eye measured in transverse direction, length = longitudinal length of the eye, width = transverse length of the eye, volume = volume of the visible part of the eye. Measurements and morphological characteristics described and used throughout the manuscript are: Fc = Facial carinae, Fv = Fastigium of vertex, Fr = Frontal ridge, Pp = Prosternal process.

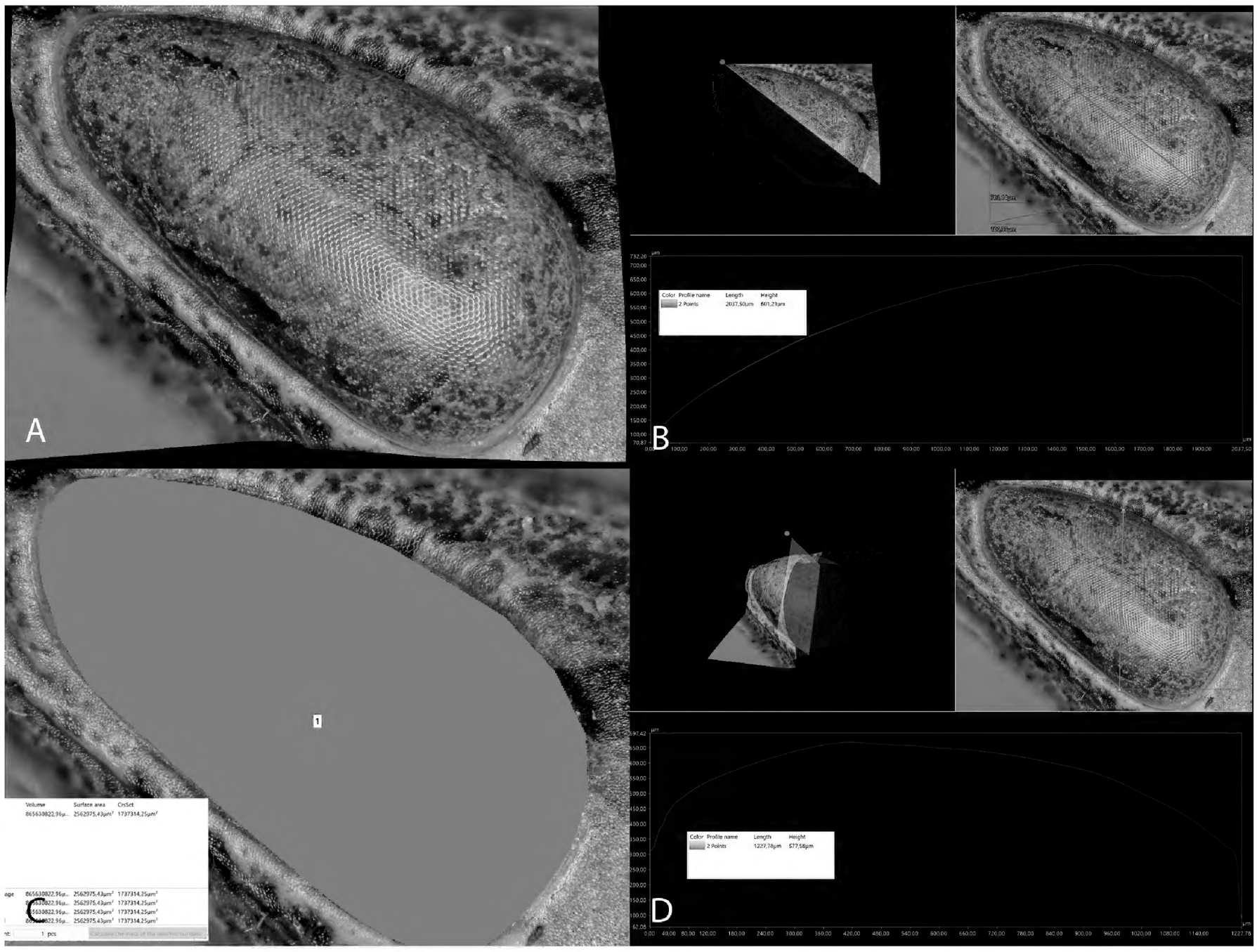

Figure 2. The outputs of 3D eye analyses in Keyence VHX 7000 using the example of *Betiscoides* specimen HLMD-Cael-379PT, B169. **A.** 3D image of the eye, ×150; **B.** The output and measurement of the longitudinal height and length of the eye; **C.** The manually drawn polygon and result window of the 3D volume measurement of the eye; **D.** The output and measurement of the cross-sectional height and width of the eye.

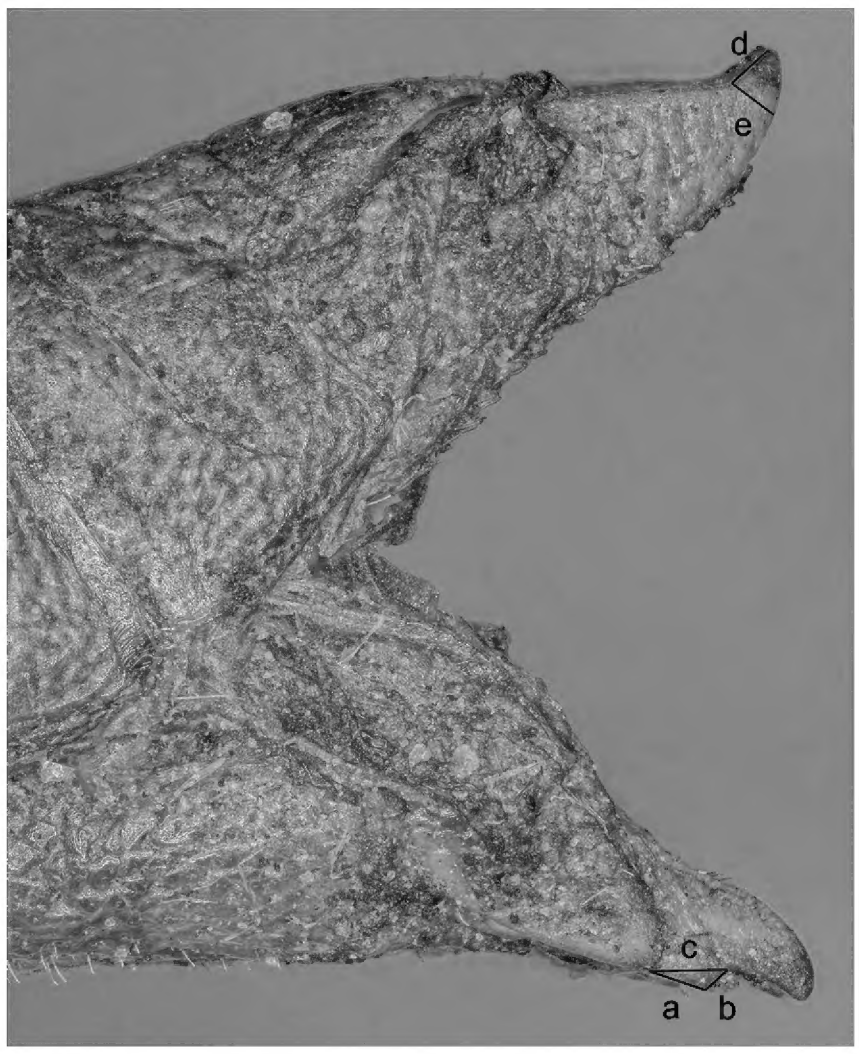

Figure 3. Showing the female genital characters using the example of *Betiscoides nova* sp. nov. specimen HLMD-Cael-8PT, B162. a = Protrusion line 1, b = Protrusion line 2, c = protrusion distance, a, b, c = protrusion, d = upper valve distance, e = upper valve width.

Nomenclature act

The electronic version of this article in Portable Document Format (PDF) will represent a published work according to the International Commission on Zoological Nomenclature (ICZ), and hence the new name contained in the electronic version is effectively published under that Code from the electronic edition alone. This published work and the nomenclatural acts it contains have been registered in ZooBank, the online registration system for the ICZN. The ZooBank LSIDs (Life Science Identifiers) can be resolved and the associated information viewed through any standard web browser by appending the LSID to the prefix http://zoobank.org/. The LSID for this publication is: 6B534FD5-542C-4636-87D1-1738CE33D9F8.

Results

Molecular analyses

Phylogenetic reconstruction with Bayesian interference showed the same relations as results obtained from Maximum Likelihood analyses. In total, sequences of 123 specimens were included in the phylogenetic reconstruction

and 24 DELs were derived confirming the lineage division revealed by Matenaar et al. (2018). The newly added sequences of the voucher specimens clustered within DEL 19 and DEL 22 respectively. The added *Betiscoides* sequences of Matenaar et al. (2016) clustered within DEL 1, 3 and 6. Overall, the BPP and Bootstrap values of the earlier splits of the main clades were higher compared to the reconstruction in Matenaar et al. (2018) meaning the addition of the specimens led to an even more robust dataset than before and confirming the phylogeny of *Betiscoides* once again (Fig. 4). Specimens of DEL 19 clustered in two subclades with a mean p-distance between these subclades of 0.0170. Specimens considered as *B. meridionalis*, *B. parva* and *B. sjostedti* (see below) clustered in DEL 3, DEL 9 and DEL 8 respectively with the highest genetic distance between *B. meridionalis* and *B. sjostedti* (p = 0.0779) and the lowest between *B. meridionalis* and *B. parva* (p = 0.0697). The overall highest genetic distance was detected between DEL 2 and 19 (p = 0.1098) and the lowest between DEL 23 and DEL 24 (p = 0.0288). The genetic distance between DEL

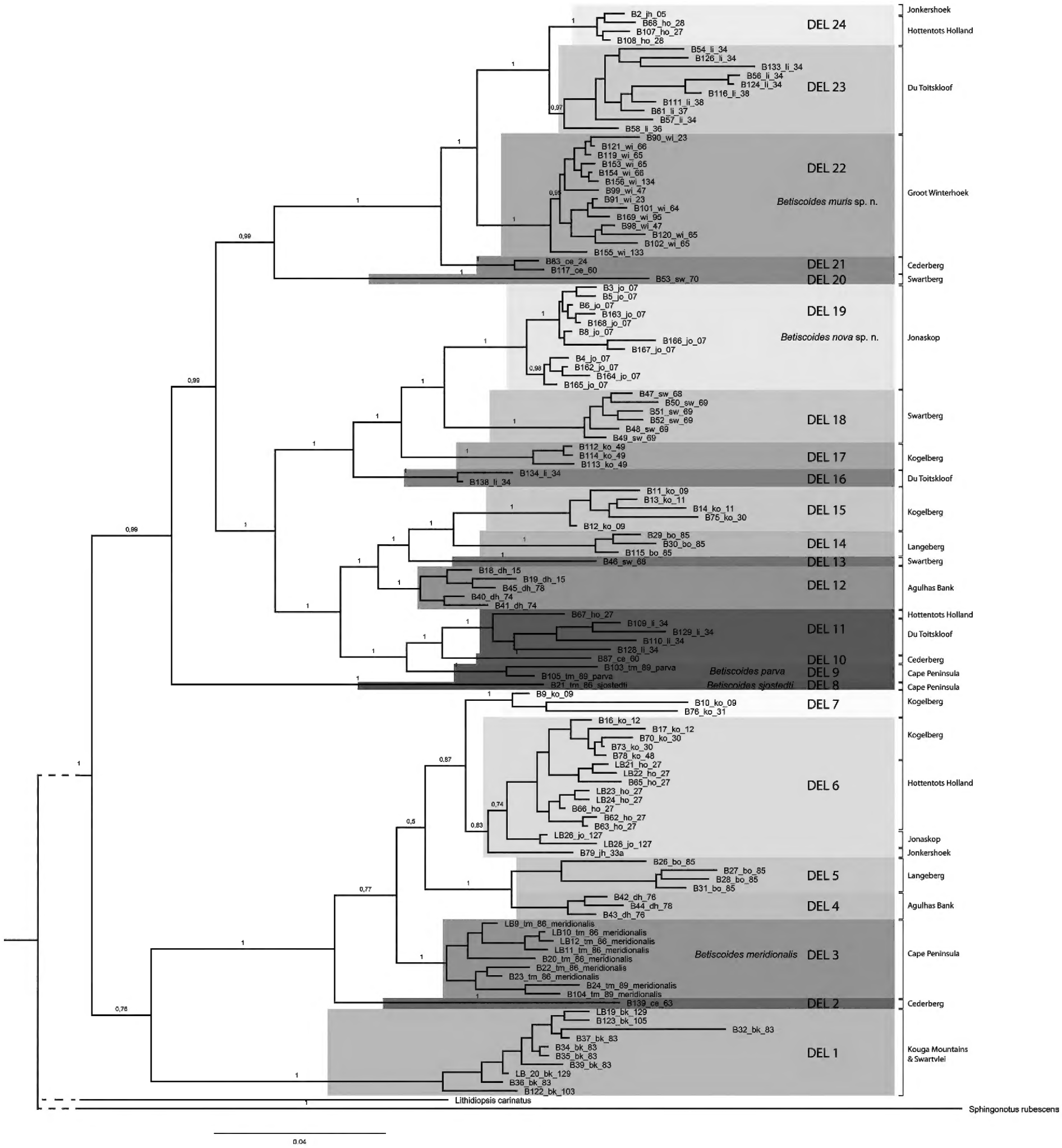

Figure 4. Consensus tree of the Bayesian Inference for genes 12S, NDS, ND5, ITS2 and H3, 2402 bp in total, 10 million generations with sample frequency of 1000. The tree is divided into 24 divergent evolutionary lineages, five of them representing valid species. The respective species are *Betiscoides meridionalis*, DEL 3, *B. sjostedti*, DEL 8, *B. parva*, DEL 9, *B. nova* sp. nov., DEL 19 and *B. muris* sp. nov., DEL22. Collection areas are signaled on the right-hand site. Jonkershoek is part of the Hottentots Holland Mountains; modified from Matenaar et al. 2017.

19 and the three nominal species of *Betiscoides* ranged between p = 0.0675 and 0.0855; the genetic distance between DEL 22 and the nominal species of *Betiscoides* ranged between p = 0.0734 and 0.080.

Morphology

The morphological examination of the collected specimens represented in the phylogenetic reconstruction revealed shared diagnostic characters when compared to the nominal species, confirming their overall allocation to the genus *Betiscoides* (body slender; head from above conical; pronotum cylindrical; anterior and middle legs short; cerci very small, straight and conical; subgenital plate elongate; female ovipositor valves recurved at the tips, not toothed, (Key 1937)). Intraspecific variability turned out to be high but certain constant differences in morphological traits between the DELs could be identified (see below). Furthermore, fine scale morphological analyses provided insights into morphological structures (shape of Pp, hairiness of the body) and the traits revealed should be added to the existing character description by Key (1937). The auto area measurement on the subgenital plate of HLDM-Cael-364HT, B156 resulted in an automatic counting of 172 extracted shapes. Except for two small grains on the subgenital plate, the counted shapes were hairs (Fig. 5). The analysis failed when applied on images of rather smooth and hairless structures and thus, results were not further used as quantitative diagnostic characters.

Taxonomic accounts

Genus *Betiscoides* Sjöstedt, 1924

Remarks. The genus *Betiscoides* Sjöstedt, 1924 was described by Sjöstedt (1924) and revised by Key (1937). Further descriptions of the morphological characters of *Betiscoides* with altered terminology followed (e.g. Dirsh 1965) and considering the new findings of this study, it is reasonable to provide a revised definition of the genus.

Definition. Type species: *Betiscoides meridionalis* Sjöstedt, 1924, type locality: South Africa. Body slender or thin, elongate, stick-like, smooth or hairy, with a prominent ventral line of hairs along the abdomen or at the end of tergits five to eight. Antennae thin or thick ensiform, segments strongly separated, finely and evenly rugose. Head in dorsal view conical. Frontal ridge compressed between antennae. Eye longitudinal or ovate and prominent. Pronotum cylindrical, with very weak or no median carina. Prosternal process trapezoid, T-shape, or lamelliformly compressed, laterally either

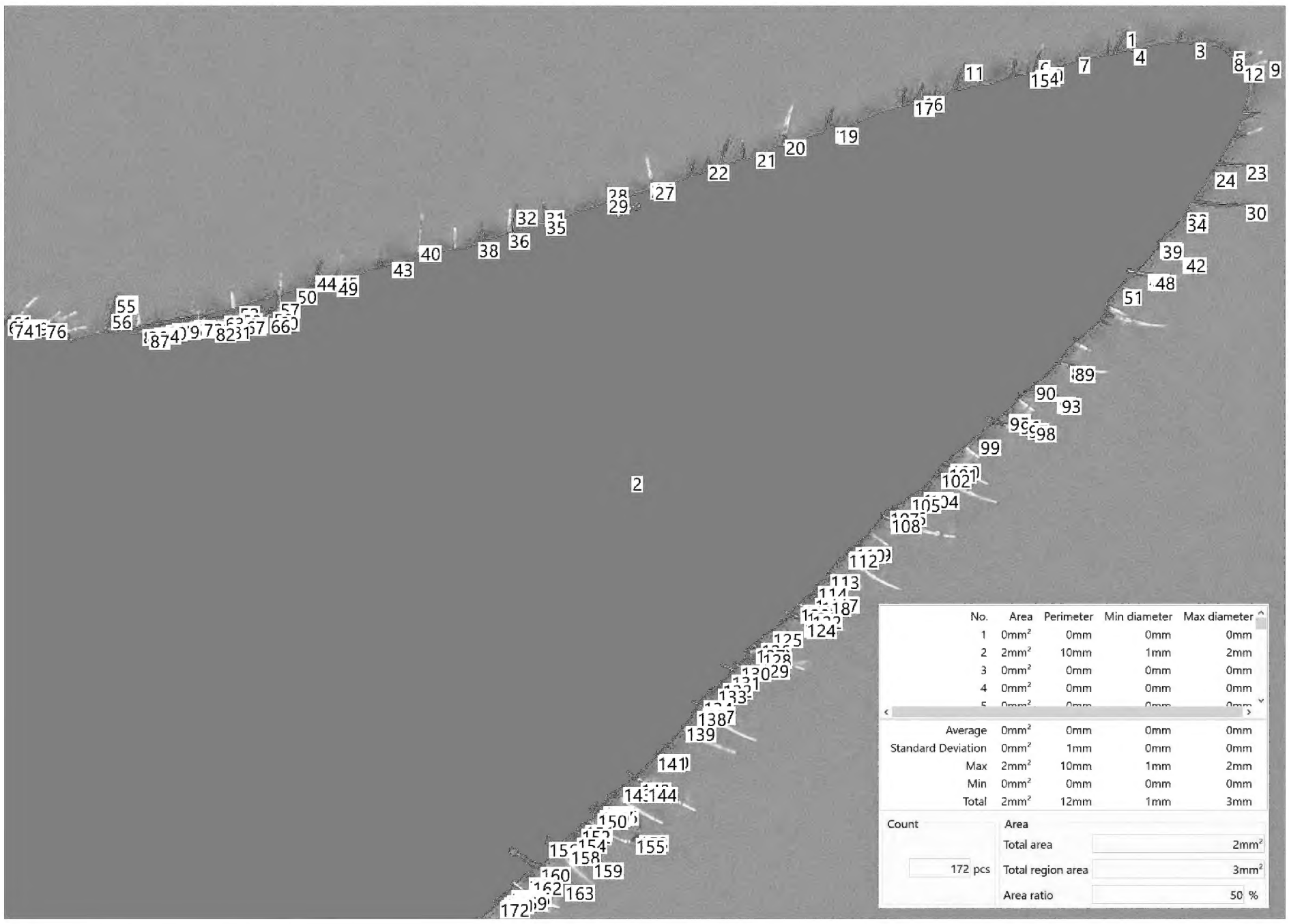

Figure 5. The extracted shape of the tip of the abdomen of *Betiscoides muris* sp. nov. specimen HLMD-Cael-364HT, B156 in the background. Keyence VHX 7000, ×150, 3D, HDR, fine scale composition and, foregrounded, the output of the automatic counting of the extracted shapes.

flat or raised in the anterior or posterior part. Mesosternal interspace reduced, mesosternal lobes connected. Abdomen with fine longitudinal, dorsal median carina. Tympanum absent. Anterior and middle legs short; sometimes hairy, hind femur slender. External apical spine present. Tarsus shorter or half the length of the tibia. Arolium large, sometimes white. Male supra-anal plate triangular in dorsal view. Cerci very small, straight and conical. Subgenital plate elongate and conical. Female ovipositor valves slightly or strongly recurved at the tips; not toothed.

A phylogenetic reconstruction revealed that the sister taxon of the genus *Betiscoides* is *Gymnidium* Karsch, 1896 (Matenaar et al. 2016). The genus *Betiscoides* contains the following species: *Betiscoides meridionalis* Sjöstedt, 1924, *B. parva* Key, 1937, *B. sjostedti* Key, 1937, *B. nova* sp. nov. and *B. muris* sp. nov. While the description of *B. meridionalis* and *B. sjostedti* remains valid concerning the hairiness of the body, the body and especially the end of the abdomen of *B. parva* is fairly hairy (Fig. 6) and thus, its character description is hereby revised. In order to extend the definition for the three known nominal species considered by Key (1937), I provide the following additional morphological characters analyzed in the specimens collected at, or very close to, the type localities of the nominal species: ratio of the eye length to the length of the fastigium, degree of the male subgenital plate, volume of the body and, volume of the visible part of the eye. In addition, I provide measurements of the "female genital characters" for *B. meridionalis*.

Betiscoides meridionalis Sjöstedt, 1924

Remarks. Specimens of DEL 3 from Cape Point, Table Mountain NP, are hereby considered as *Betiscoides meridionalis* as they coincide with its overall morphological diagnostic characters. The large and slender body, the 24-jointed, ensiform, antennae, the very elongate head with the Fv nearly twice the length of the eye as well as the extremely elongate and acutely pointed subgenital plate, reason this allocation. The specimens occur in sympatry with the specimen from DEL 8.

Material. Male. HLMD-Cael-380, LB11, Genbank Acc: KU206332, KU214602, 34°19'2.30"S, 18°25'12.66"E, 42 m above sea level, South Africa, Western Cape, Table Mountain National Park, Cape Point, Restio wetland, November 2013, L. Bröder leg.

Vol: 88.3974 mm^3 or 8.83974e-08 m^3; Vol. eye: 1002540337.66 μm^3, ratio eye length/ fastigium length: 1.30, Subgenital plate degree: 31.6°

Female. HLMD-Cael-383, B24, Genbank Acc: MG243742.1, MG244116.1, MG243841.1, MG243940.1, MG244036.1, 33°57'32.18"S, 18°23'16.06"E, South Africa, Western Cape, Table Mountain National Park, Twelve Apostle, Restio wetland, March 2012, S. Wirtz leg.

Upper valve degree: 52°, upper valve distance = 182 µm, upper valve width = 201 µm, protrusion degree = 129°, Pr line 1 = 146 µm, Pr line 2 = 75 µm, Pr distance = 205 µm, Pr distance to tip of the dorsal valve = 280, 11 µm, Pr vertical distance = 78 µm, Pr straight-lined, apex acute.

Betiscoides parva Key, 1937

Remarks. Specimens of DEL 9 from the 12 Apostles, Table Mountain NP, are hereby considered as *Betiscoides parva* as they coincide with its overall morphological diagnostic characters. The small body size, the thick ensiform shape of the antennae and the large, prominent and ovate eyes, as well as the relatively large feet (half the length of the hind tibiae), reason this allocation. In order to assess the hairiness, the specimens of DEL 9 were compared with images of the holotype (male, NHMUK Cape Peninsular, South Africa, December 1930), both showed fairly hairy integument. In order to assess the female genital characters, I analyzed images of the allotype (female, NHMUK, Cape Peninsular, South Africa, December 1930).

Material. Male. HLMD-Cael-381, B103, GenbankAcc: MG243794.1, MG243893.1, MG243991.1, MG244078.1, MG244168.1, 33°57'32.18"S, 18°23'16.06"E, South Africa, Western Cape, Table Mountain National Park, Twelve Apostle, Restio wetland, March 2012, S. Wirtz leg.

Vol: 42.080 mm^3 or 4.20806e-08 m^3; Vol. eye: 973202045.68 μm^3, ratio eye length/ fastigium length: 0.54, Subgenital plate degree: 51° rounded.

Betiscoides sjostedti Key, 1937

Remarks. The specimen of DEL 8 from Cape Point, Table Mountain NP, is hereby considered as *Betiscoides sjostedti* as it coincides with its overall morphological diagnostic characters. The intermediate body size, the almost equal length of the antennae and head, the fastigium about 2/3 the length of the eye, as well as the comparatively short subgenital plate, reason this allocation. In order to assess the hairiness, the specimen of DEL 8 was compared with images of the holotype (male, NHMUK, Table Mountain, South Africa, December 1929–1930), both showed fairly smooth integument. This specimen occurs in sympatry with specimens from DEL 3. In order to assess the female genital characters, I analyzed images of the allotype (female, NHMUK, Table Mountain, South Africa, December 1929–1930).

Material. Male. HLMD-Cael-382, B21, Genbank Acc: MG243739.1, MG243838.1, MG243937.1, MG244033.1, MG244113.1, 34°19'2.30"S, 18°25'12.66"E, 42 m above sea level, South Africa, Western Cape, Table Mountain National Park, Cape Point, Restio wetland, March 2012, S. Wirtz leg.

Vol: 58.9269 mm^3 or 5.89269e-08 m^3; Vol. eye: 773244697.52 μm^3, ratio eye length/ fastigium length: 0.78, Subgenital plate degree: 40.8°. The three nominal species are shown in Fig. 6.

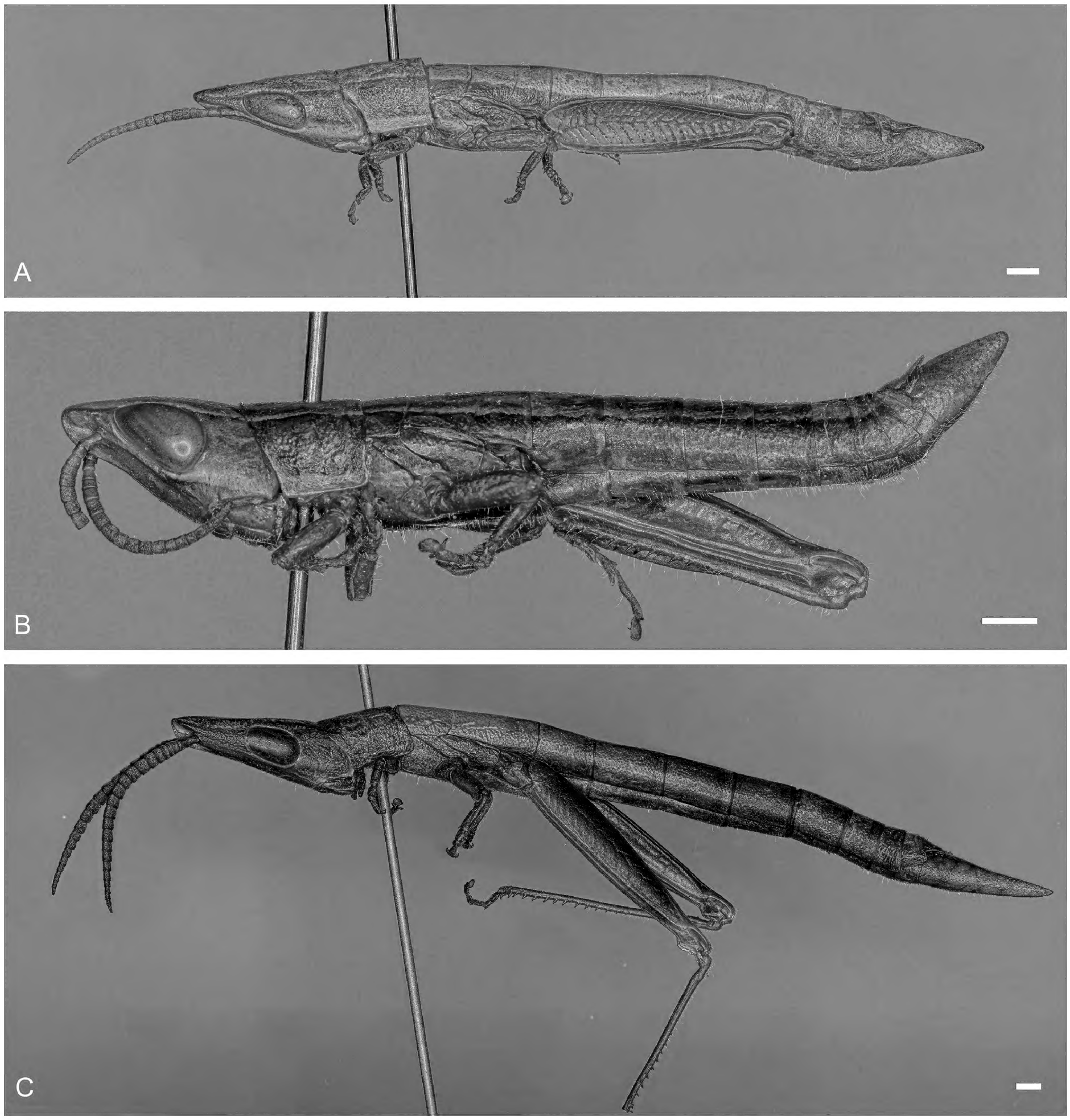

Figure 6. Overview of the nominal species of *Betiscoides*. **A.** *B. sjostedti*, HLMD-Cael-382, B21, DEL8; **B.** *B. parva*, HLMD-Cael-381, B103, DEL 9, and **C.** *B. meridionalis* HLMD-Cael-380, LB11, DEL 3. Specimens were collected at or close to the respective type localities. Scale bars: 1 mm.

Betiscoides nova sp. nov.

https://zoobank.org/E6FCA740-2659-4337-8557-06D602D6252A

Type material. The type material is deposited in the invertebrate collection of Hessisches Landesmuseum Darmstadt (HLMD). ***Holotype.*** Male, pinned. HLMD-Cael-4HT, B168, Genbank Acc. PP417675, South Africa, Western Cape province, Jonaskop, 33°58'9.75"S, 19°30'17.99"E, 1553 m above sea level, Plot 07, Restio wetland, 13 Dec 2013, leg. L. Bröder, E. Heym & D.Matenaar, ***Paratypes.*** Allotype. Female, pinned. HLMD-Cael-18AT, B166, paratypes HLMD-Cael-5-19PT, all same data as holotype. In total, five female and ten male paratypes are designated.

Etymology. The specific epithet is a Latin adjective (feminine form) meaning 'extraordinary' or 'new'. It refers to the species' prominent habitus and to the fact that it is a new species characterized with the help of novel techniques.

Definition. The described species is assigned to the genus *Betiscoides* Sjöstedt, 1924 due to its phylogenetic position and overall morphological characteristics. The species is defined by the elongate, stick-like medium to large sized body, ensiform antennae, which are triangular in cross-section; its conical head, which is in profile al-

most equal in length and height, large eyes, the trapezoid shape of the prosternal process with two kinds of hairs and little variation in general. The end of the abdomen has only few and short hairs. The arolium is very large. The subgenital plate is elongate and conical; the ovipositor is short with robust, recurved valves.

Diagnosis. This new species differs morphologically from the described ones mostly through its robustness and higher body volume and the almost identical HL and HH. The body is less elongate than *Betiscoides meridionalis*. Genital valves are less acute compared to *Betiscoides meridionalis*. Furthermore, the new species represents a divergent evolutionary lineage (DEL 19) as stated in Matenaar et al. (2018) and is genetically distinct representing the closest relative of *B. parva* (p-distance: ~ 0.067). As Key (1937) stated for *B. parva* and *B. sjostedti*, also this species is far less elongate than *Betiscoides meridionalis*, and *B. parva*, *B. nova* and *B. sjostedti* seem morphologically more related to another than any of these to *B. meridionalis*. In general, the new species seems to be morphologically intermediate between *B. parva* and *B. sjostedti*, whereby the robustness is more similar, to *B. sjostedti* but regarding the general coloration of the body, the shape of the Fr, the large eyes and the angularity of the end of the abdomen, there is a resemblance with *B. parva*, although *B. nova* is smooth, whereas *B. parva* is hairy. Furthermore, *B. nova* lacks the big feet of *B. parva* (Figs 7, 8).

Description of the holotype. Body robust, of medium size (Figs 9A, 10A). BL 25.81 mm, Integument finely rugose, shiny, smooth. Body of type specimen curved to the right in dorsal view, starting at the 10th tergit. Antennae 22-jointed, ~ 4.5 mm, ensiform, slightly flattened above and slightly tapering, in length longer than the head, reaching the pronotum, evenly punctured, grooves darker than the rest, fine hairs, end of each segment lined in lighter ground color. HL 3.82 mm, HDL 6.13 mm, HH 3.77 mm, head from above elongate, conical, from above app. 1.5 as long as its width at the occiput. Fv 1.6 mm, 0.78 the length of an eye, angular, the margins well raised but obtuse-angled, margins of contrasting color, forming a thin, dark brown line, narrowing from the anterior margin of the eye forwards, protruding in front of the eyes culminating at the tip of the vertex as a protruding dot. Median carinula faintly discernible on the fastigium. Head in profile very slightly concave above, face slightly incurved, angle acute (app. 57.9°). Apex of fastigium in profile slightly raised; frons oblique. Fr between the antennae in profile somewhat projecting, thin, lamelliform, lateral carinae below the antennae very narrow, shallowly sulcate, in basal part obliterated. Fc straight, distinct throughout. Eyes ovate, about twice as long as their maximum width, their surface strongly convex, both margins somewhat curved, the upper more so than the lower, lower margin slightly raised, as of callus. Ratio of eye length and fastigium length 0.60. PL 3 mm. Pronotum cylindrical, with weak median and indistinct lateral carinae; no sulcus crossing dorsum. Hind margin of metazona very slightly concave, anterior margin straight; sides of pronotum with the lower margin almost straight, sloping downand forwards in the anterior part, posterior margin practically straight, anterior lower angle slightly more than 90°, rounded; posterior lower angle 90°, rounded. Pp trapezoid, about twice as long as broad, its margins and angles rounded, the anterior end little broader than the posterior, finely haired and rugose (anterior width: 299.27 µm, posterior width: 263.23 µm, length ~ 492 µm), see Fig. 11A. Mesosternal interspace reduced/ closed with mesosternal lobes connected. Metasternal interspace like a pigs' nose. Anterior and middle legs strongly shortened. Carinae of anterior and middle femora with fine and sparse hairs, anterior and middle tibiae and tarsi hairy, HFL 9.47 mm, hind legs reaching beyond the end of abdomen. Hind femora robust, about five times as long as their maximum width, upper carina of femur finely toothed as of small frequent tubercles, hind tibiae with 8 outer and 10 inner spines. External apical spine of hind tibia present. Hind tarsus shorter than half of the length of the tibia. Arolium very large and of white color. Supra-anal plate elongate, 1.33 mm, acutely angular. Cercus short, conical. Supra-anal plate with the basal part about one third the length of the apical part, the longitudinal depression distinct; the apical part of the plate shaped like an equilateral triangle with the base curved and the sides straight; apical angle widely rounded; no depression on the apical angle. Subgenital plate acute and elongate (angle app. 50°), but apex rounded, comparatively sharply pointed in dorsal view, lower margin convex, upper margin straight. Outer genitalia only sparsely haired with the subgenital plate featuring a fine line of hairs along the fold. Genital apparatus about the length of 2.5 tergits. SGP: 2.33 mm, three tergits: 3.35 mm ratio: 0.6955. The total body volume is 1.33029e-07 m^3 (133.029 mm^3). The volume of the visible part of the eye is 1160104343.13 µm^3, the longitudinal height being 540.54 µm, and the length 2339.22 µm. The cross-sectional height is 657.29 µm and the width itself is 1372.3 µm. General coloration deep -brown. Antennae, fore and middle legs and knees are slightly paler than the brown primary color of the body. The upper part of the head, thorax and abdomen, within the callus line, is of green color. A longitudinal shallow stripe extends from the front of the head backwards along the central ridge of the body. The second and third tergit show brown markings between the callus lines; the posterior part of each tergit is of brown color, like a thin line, starting at the 5th tergit. The lateral stripe backwards from the base of the eye is beige-white. It starts at the lower hind corner of the eye (as a somewhat raised callus ridge) and stops right behind the middle leg. Eyes brown, anterior femora reddish-brown, middle femora green, tibia and tarsi dark brown, hind femora of the same green as the dorsal part, knees and upper and lower external carina of the hind femur pale brown. Hind tibia brown and very dark in the lower side, spines and spurs black-tipped.

Description of the allotype. Larger than the male (Fig. 7E). BL 30 mm, HL 5 mm, HDL 7 mm, HH 3.79 mm, Head in profile straight, angle acute (app. 57.5°). Antennae 22-jointed, 5.5 mm, ensiform, finely punctured. Fr strongly protruding, lateral carinae of frontal ridge dis-

tinct beneath the sulcus, almost until clepeus. Fastigium 0.6 the length of an eye. PL 3.7 mm, sides of pronotum with lower margin straight; anterior margin sloping forward, only very slightly incurved, posterior margin slightly incurved, sloping forward in the upper part. Anterior lower angle more than 90°, posterior lower angle 90°, both rounded. Pp trapezoid, slightly resembling the number 8, rugose and finely haired with two different kinds of hair, margins rounded, the anterior part slightly broader than the posterior (anterior width: 297.32 µm posterior width: 212.37 µm, length: ~ 562 µm; measured in tilted angle (see Fig. 12). HFL 10.5 mm, hind tibiae with 10 outer and 12 inner spines, black tipped. Genital valves recurved, rounded in the apical part, hairs inside.

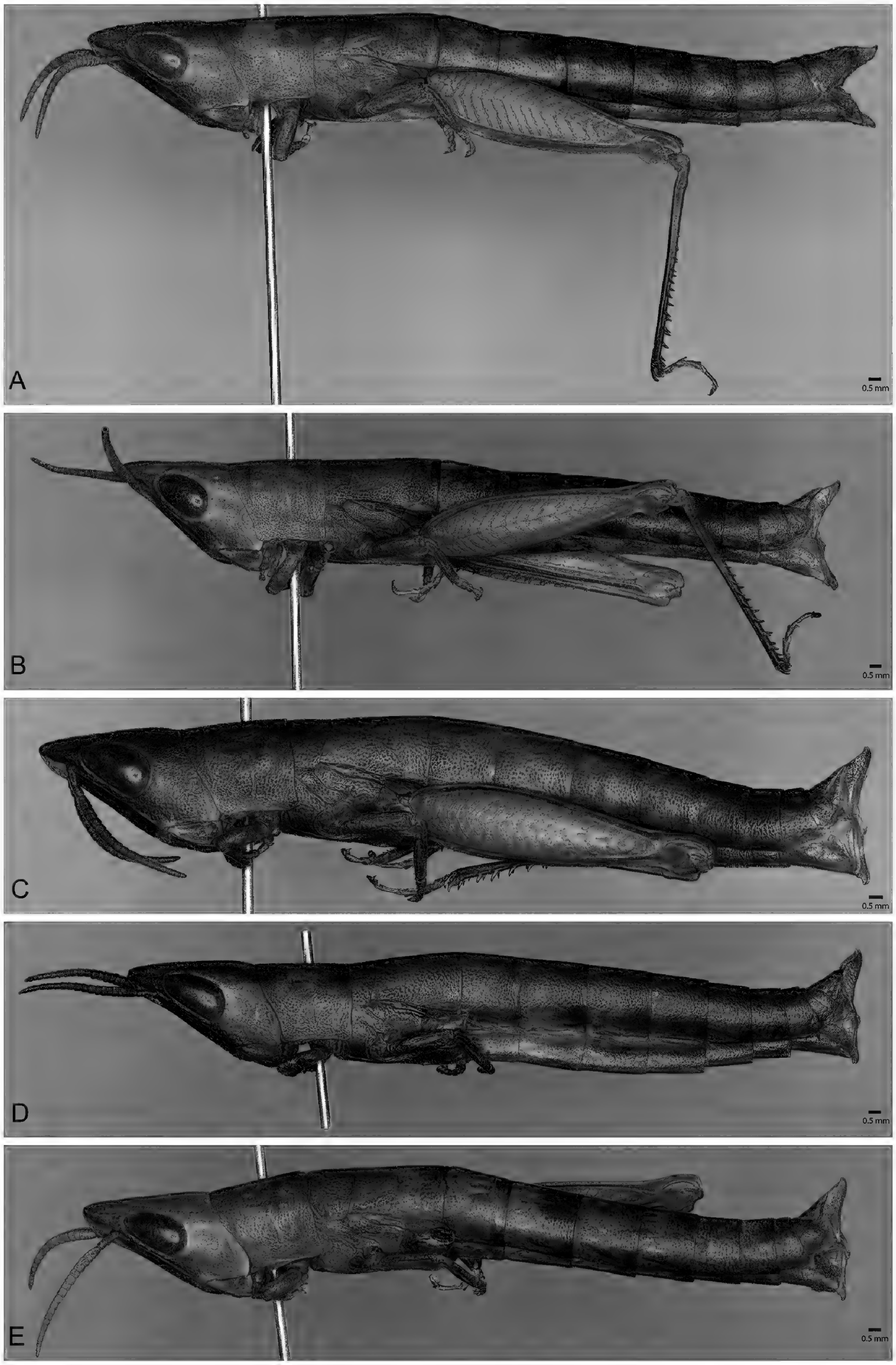

Figure 7. Lateral views of female allo- and paratypes of *B. nova* sp. nov. **A.** HLMD-Cael-8PT, B162; **B.** HLMD-Cael-16PT; **C.** HLMD-Cael-12PT; **D.** HLMD-Cael-14PT, B165; **E.** HLMD-Cael-18AT, B166. HLMD-Cael-18AT is the allotype.

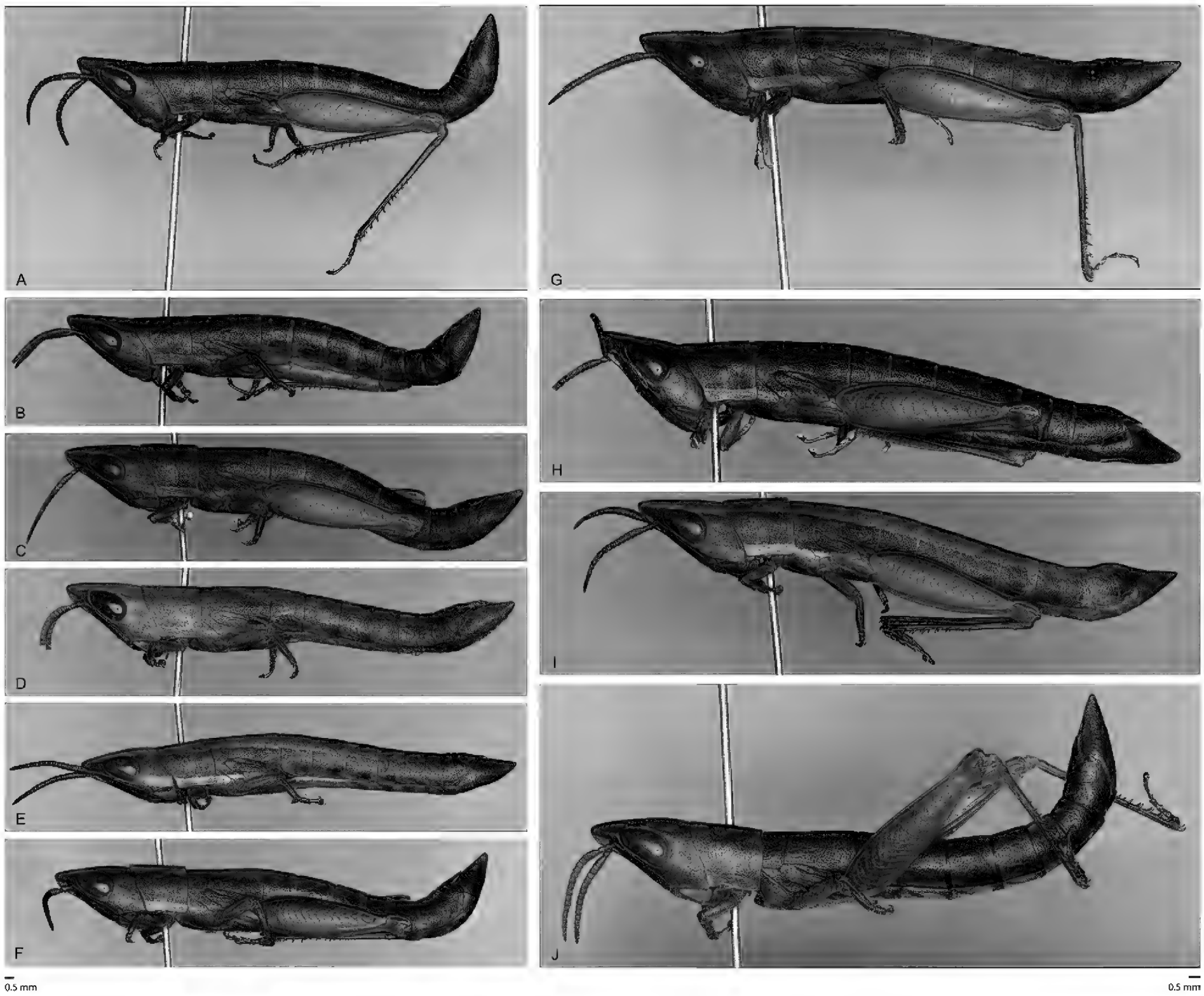

Figure 8. Lateral views of the paratypes of *B. nova* sp. nov. **A.** HLMD-Cael-7PT; **B.** HLMD-Cael-15PT, B167; **C.** HLMD-Cael-9PT; **D.** HLMD-Cael-6PT; **E.** HLMD-Cael-10PT, B163; **F.** HLMD-Cael-19PT; **G.** HLMD-Cael-11PT; **H.** HLMD-Cael-17PT; **I.** HLMD-Cael-5PT; **J.** HLMD-Cael-13PT.

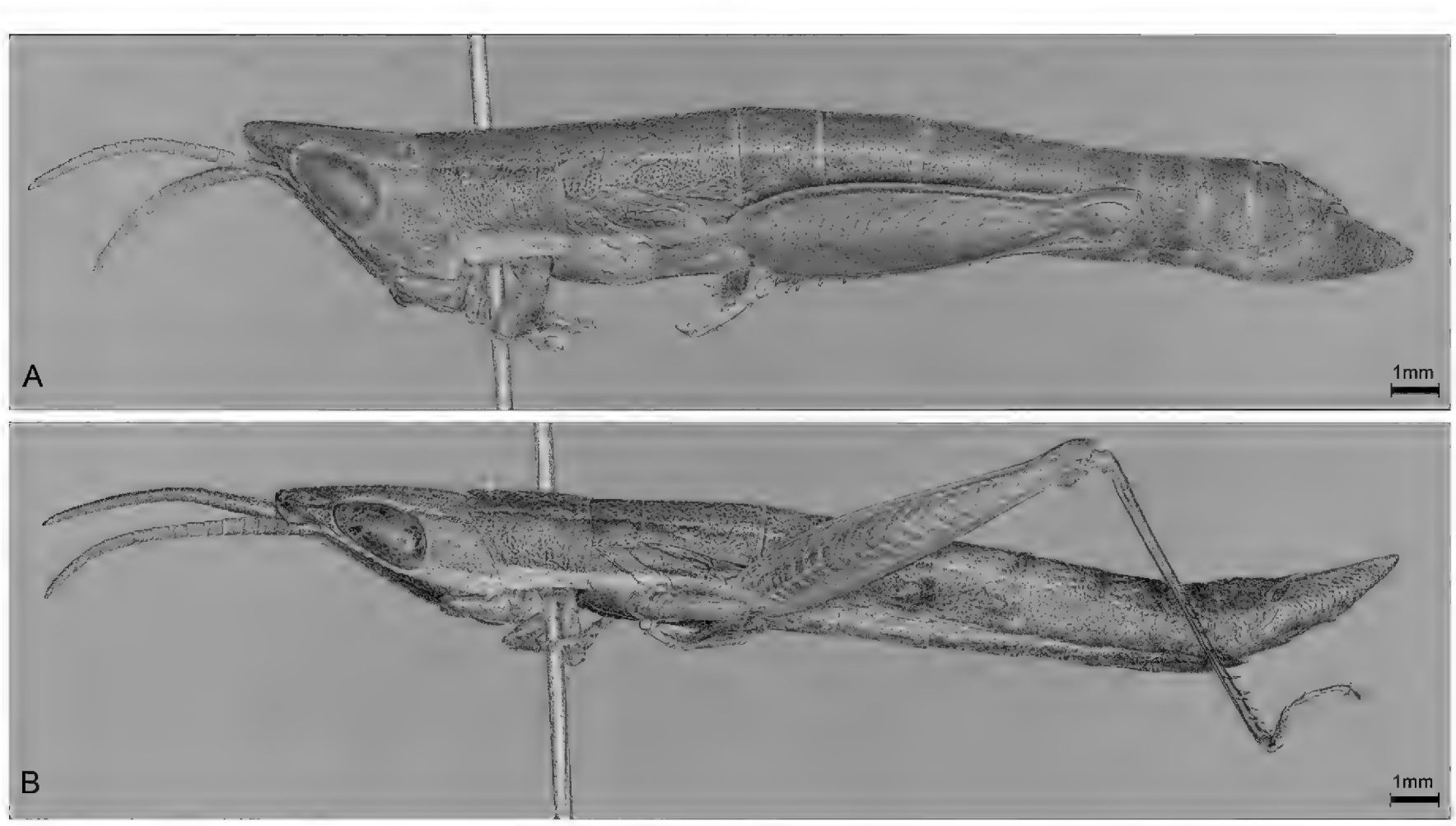

Figure 9. Holotypes of *Betiscoides nova* sp. nov. and *Betiscoides muris* sp. nov. in lateral view. **A.** Shows *B. nova*, HLMD-Cael-4HT, B168; **B.** Shows *B. muris*, HLMD-Cael-364HT, B156.

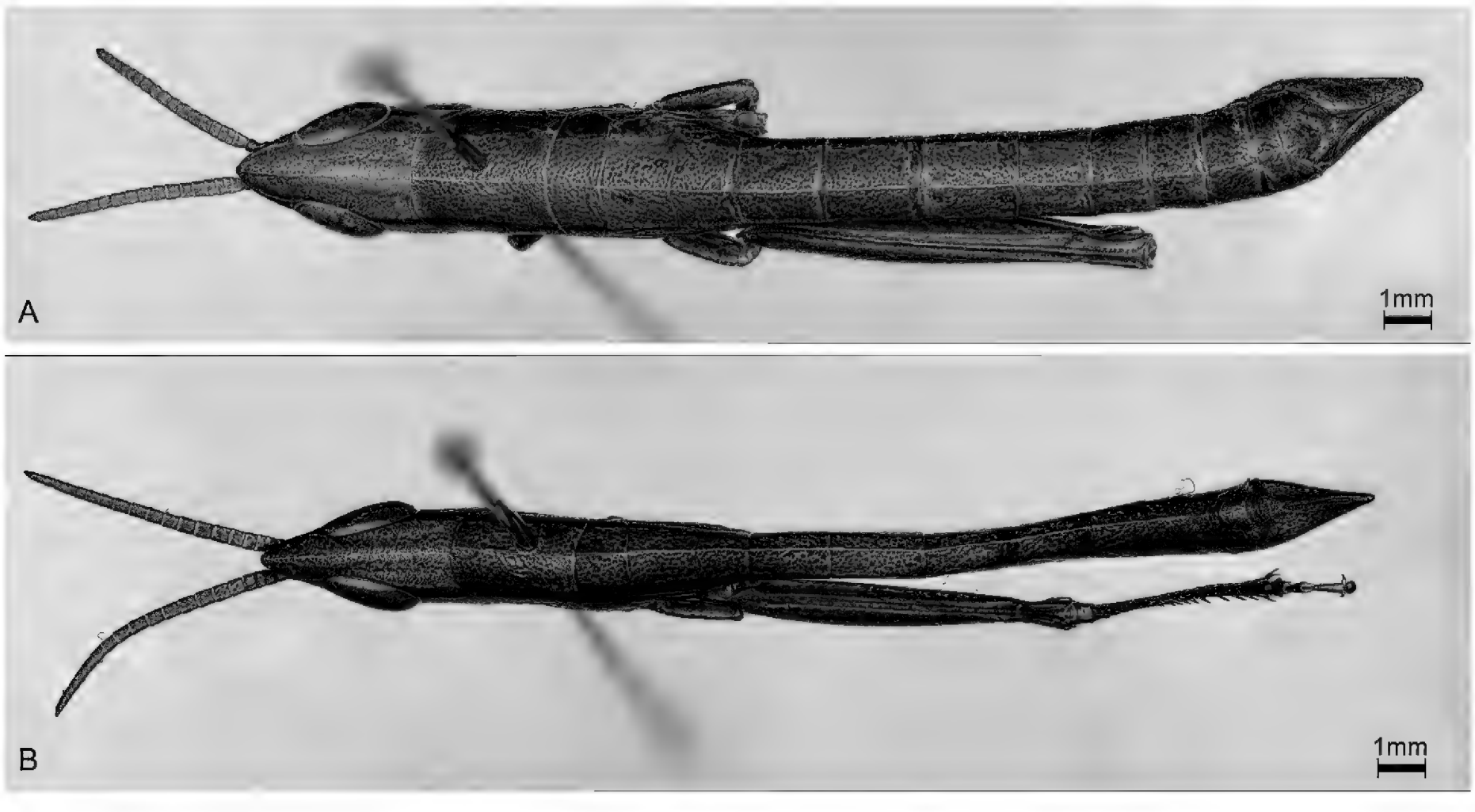

Figure 10. Holotypes of *Betiscoides nova* sp. nov. and *Betiscoides muris* sp. nov. in dorsal view. **A.** Shows *B. nova*, HLMD-Cael-4HT, B168; **B.** Shows *B. muris*, HLMD-Cael-364HT, B156.

Supra-anal plate 1.4 mm in total, subgenital plate acute. Genital valves spread. Substrate on the lower valves. Degree of protrusion acute (124°), Pr line 1 slightly longer (174 µm) than Pr line 2 (109 µm), Pr distance is 253,15 µm, Pr area is of 13755.38 μm^2 and protrusion vertical distance to tip is 180.92 µm. Protrusion to tip of valve distance is 311.02 µm. Upper valve degree acute of 163°, short upper valve distance: 239 µm, upper valve width 311 µm (see Fig. 13A). General coloration brown, in dorsal view head greenish brown, pronotum and abdomen colored in mixture of orange-brown, greenish brown, end of abdomen dark brown. Ventral ridge of the body finely but densely haired, head and hind femur of yellow-green color, knee and beginning of hind tibia pale brown, apically slightly darker, arolium large and white; black claws. The volume of the visible part of the eye is 1729519566.68 μm^3. With the longitudinal height being 642.85 µm, and the length 2737.3 µm. The cross-sectional height is 646.17 µm and the width itself is 1412.78 µm.

Variation. Specimens show little differences in the shape of the head in profile, varying from described morphology of the holotype to a slightly more convex form. By contrast, the face differs concerning the distinction of the lateral carinae below the sulcus and the shape of the sulcus itself. In some specimens, the lateral carinae are distinct throughout, also beneath the sulcus. The sulcus is shaped as a mustache sometimes. Median Carina/ Central ridge of the body: Whereas the median carina is present in all specimens, the central ridge of the body is clearly distinct in males on the abdomen, starting on the third segment. This pattern is truly sex specific. Females show a distinct median carina throughout, but in three females (HLMD Cael-18AT, B166; HLMD-Cael-14PT, B165; and HLMD-Cael-16PT) the median carina culminates in a black spot at the verge of the fastigium of vertex. The prosternal process was described as laminate or lamelliform compressed by Key (1937) and Dirsh (1965). In contrast to the other known *Betiscoides* species, the Pp of *B. nova* can be described as trapezoid with vague variability towards a square shape. In 2D some specimens seem to show a proximal concave Pp (see Fig. 11B). Detailed 3D image analysis revealed a straight but rugose progression of the surface of the Pp (see Fig. 14). The curve progression showed a gradient of ~ 54 µm (HLMD-Cael-10PT, B163, see Fig. 14). Supra-anal plate and subgenital plate more elongate than in the holotype. Variation in spines on the hind tibia: In male, the hind tibiae had 8–9 outer and 10–11 inner spines. In females the hind tibia showed 9–10 outer spines and 11–12 inner spines. General coloration in males dark-brown. Antennae, fore and middle legs are of the same brown primary color as the body. The upper part of the head, thorax and abdomen, within the callus line, is of light brown or green color. When of green color, sometimes the hind margin of each segment of the abdomen is of light brown or orange color. Eyes brown. Hind femora pale, especially when light brown within the callus line; or green, both inside and outside, except the carina, which is sometime black-tipped, herring bone pattern distinct. Knees light brown. Hind tibiae brown and very dark in the lower side, spines and spurs black-tipped. Female: General primary coloration similar to, but slightly less dark than, that of the male. No variation toward green or light brown color within the callus line. Hind femora, both outside and inside, paler than the rest of the body, varying in one female towards yellow-green, herring bone pattern distinct, hind tibiae darker apically than basally. Detailed measurements are provided in Table 1.

The longitudinal height cannot be safely derived from the measurements since most of specimens eyes have

Figure 11. Prosternal proceses, ×200. **A.** Holotype of *B. nova* sp. nov., HLMD-Cael-4HT, B168; **B.** Shows the Pp of HLMD-Cael-10PT, B163 (*B. nova*) in ventral topview.

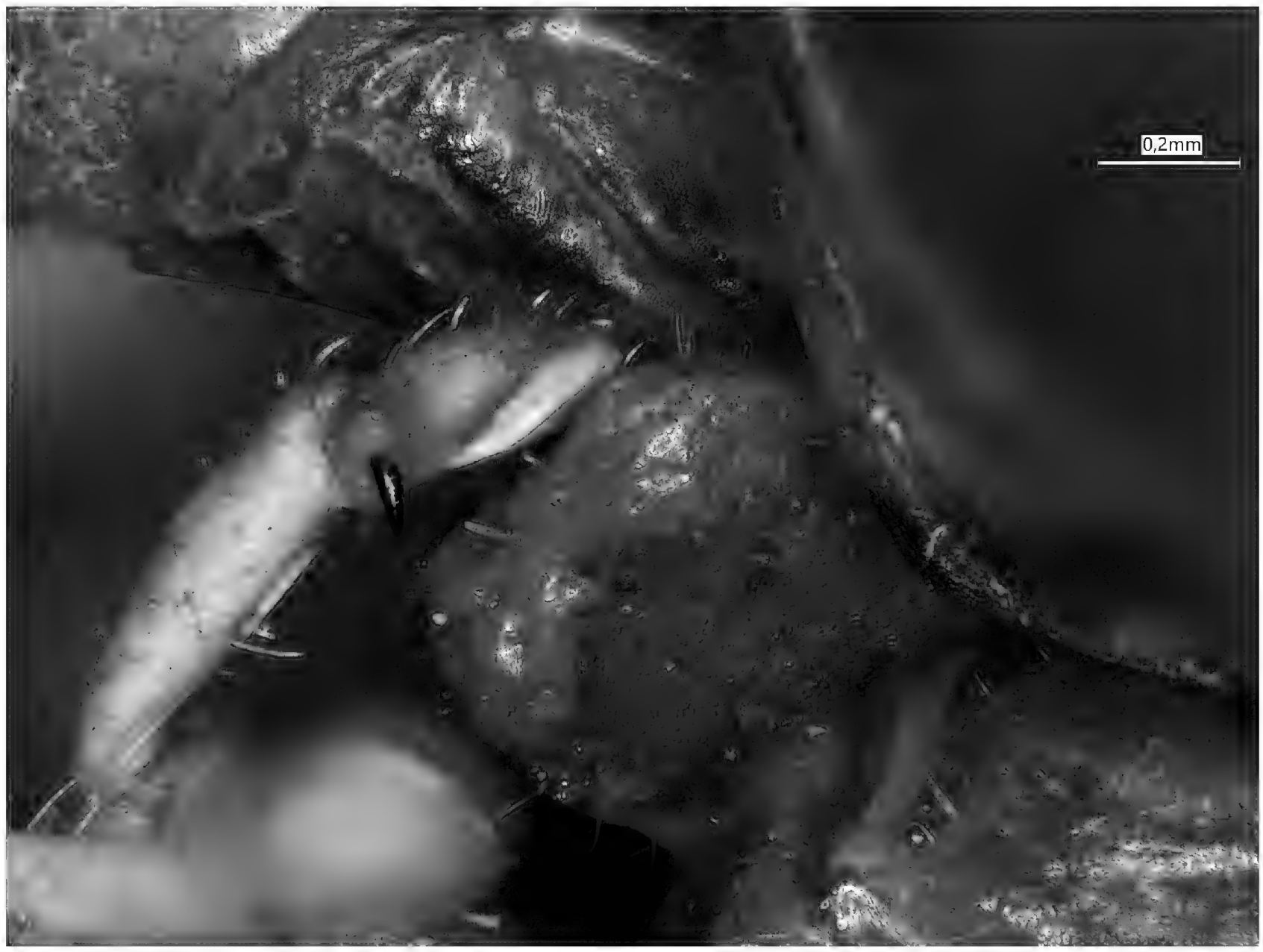

Figure 12. Image of the prosternal process of the allotype of *Betiscoides nova* sp. nov., HLMD-Cael-18AT, B166, ×200, captured in ventral view, with a tilt angle of 60°.

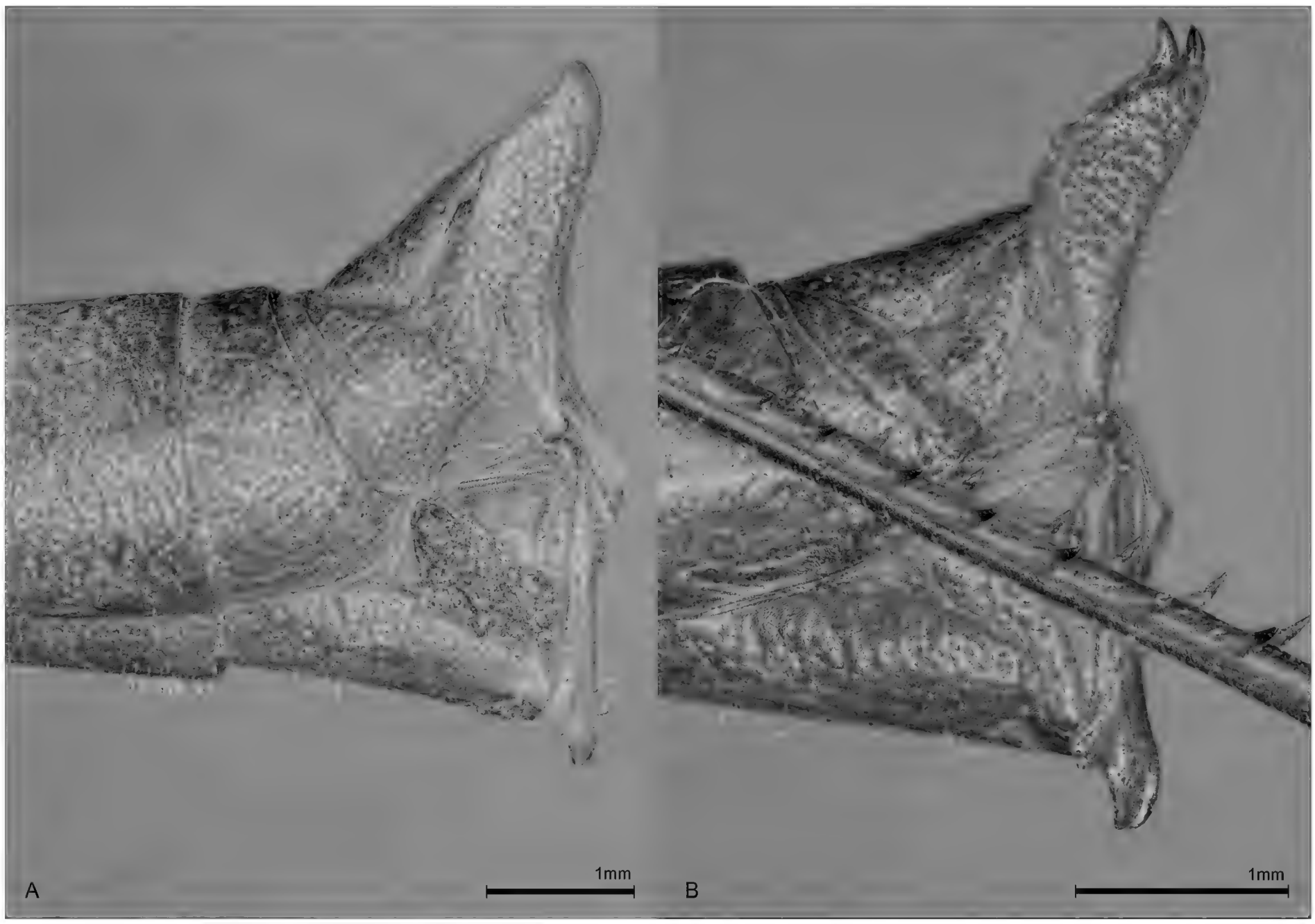

Figure 13. Ovipositor valves, lateral view. **A.** Allotype of *B. nova* sp. nov. HLMD-Cael-18AT, B166; **B.** Allotype of *B. muris* sp. nov. HLMD-Cael-368AT, B155.

been subject to certain degree of decay, which caused the highest part of the eyes to collapse at the highest point. Specimens HLMD-Cael- 6, 8, 9, 13, and 15PT were excluded from the cross sectional height analysis since the eyes had collapsed.

Distribution, ecology and conservation status. Described from 11 males and five females from Jonaskop, Western Cape, South Africa, 2013. The species occur on top of Jonaskop in restio-dominated wetland. Abundant in patches with water covering the bare ground between the single restio plants. As the three formally recognized species of *Betiscoides* are considered endangered (Hochkirch 2012a, 2012b, 2012c), I propose this status as well for *B. nova* because itis only known from a single locality and its habitat is in decline.

Betiscoides muris sp. nov.

https://zoobank.org/31D0E590-5DB8-46B2-829D-95A5EE822F42

Type material. The type material is deposited in the invertebrate collection of Hessisches Landesmuseum Darmstadt (HLMD). ***Holotype.*** Male, pinned, HLMD-Cael-364HT, B156, (Genbank Acc. PP411598, PP417668), South Africa, Western Cape province, Groot Winterhoek Wilderness Area, 32°59'21.52"S, 19°3'26.84"E, 991 m above sea level, Plot 134, Restio wetland, 18 April 2016, leg. D. Matenaar.

Paratypes. Allotype. Female, pinned. HLMD-Cael-368AT, B155, South Africa, Western Cape, Groot Winterhoek Wilderness Area, 32°59'53.06"S, 19°4'12.40"E, 929 m above sea level, Plot 133, Restio wetland, 18 April 2016, D. Matenaar. Paratypes. HLMD-Cael-362PT, B153; HLMD-Cael-366PT, South Africa, Western Cape, Groot Winterhoek Wilderness Area 32°59'35.34"S, 19°3'32.90"E, 969 m above sea level, Plot 65, Restio wetland, 18 April 2016, D. Matenaar. HLMD-Cael-363PT; HLMD-Cael-367PT, B154, South Africa, Western Cape, Groot Winterhoek Wilderness Area, 32°58'54.76"S, 19°3'18.37"E, 1001 m above sea level Plot: 66, Restio wetland, 18 April 2016, D. Matenaar. HLMD-Cael-365PT South Africa, Western Cape, Groot Winterhoek Wilderness Area, 32°59'53.06"S, 19°4'12.40"E, 929 m above sea level, Plot 133, Restio wetland, 18 April 2016, D. Matenaar. HLMD-Cael-360PT, HLMD-Cael-361PT; HLMD-Cael-369PT, South Africa, Western Cape, Groot Winterhoek Wilderness Area, 134: 32°59'21.52"S, 19°3'26.84"E, 991 m above sea level, Plot 134, Restio wetland, 18 April 2016, D. Matenaar. HLMD-Cael-379PT, B169, South Africa, Western Cape, Groot Winterhoek Wilderness Area, Restio wetland 33°0'11.81"S, 19°4'20.91"E, 908 m above sea level, Plot 95, Restio wetland, 06 March 2020, D. Matenaar. In total, five female and five male paratypes are designated.

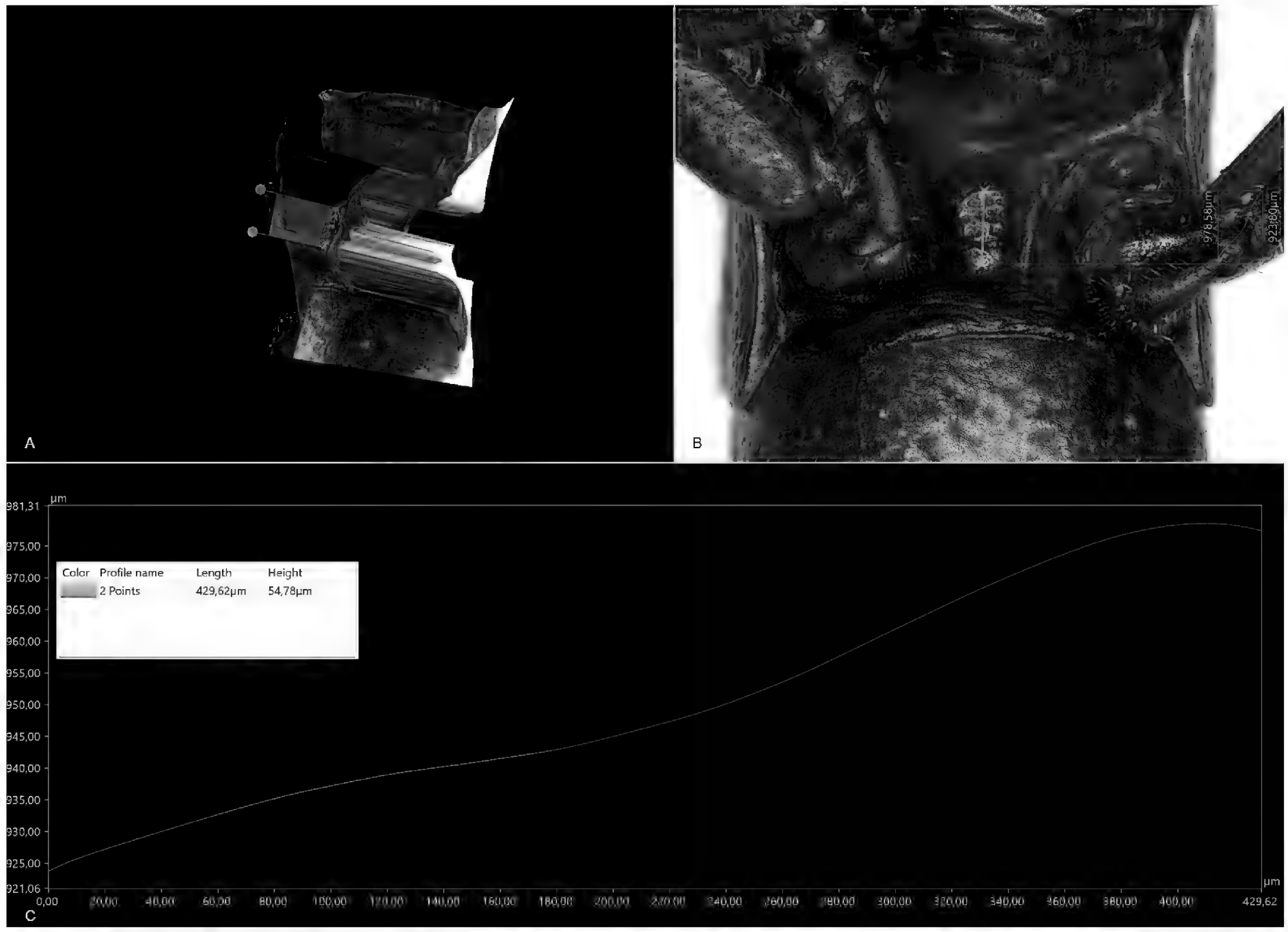

Figure 14. 3D image profile analysis of the prosternal process of specimen HLMD-Cael-10PT, B163 (*B. nova* sp. nov.). **A.** Shows the 3D image turned to profile view and the two points set to measure the distance and height progression curve of the selected part; **B.** Shows the depth image composition of the 3D image and the two points set to measure the distance; **C.** Shows the profile analysis results, including the length and height and the curve progression.

Table 1. Plane and 3D measurements of the morphological characters for males and females of *Betiscoides nova* sp. nov. and *B. muris* sp. nov.

Measurements	*B. nova* males	*B. nova* females	*B. muris* males	*B. muris* females
Body length mm	22.5–27.2	29.3–30.02	21.2–24.3	26.15–29.5
Pronotum length mm	3.0–3.3	3.5–3–7	2.2–2.65	2.85–3.4
Hind femur length mm	8.7–10	9–11	6.9–8.1	8.9–10.4
Antenna segment no.	21	21	21–22	22–23
Head length mm	3.6–4.5	4.2–5	3.5–4.3	4.3–4.7
Head diagonal length mm	5.51–6.32	6.48–7.02	4.73–5.52	5.65–6.62
Head height mm	3.26–3.77	3.69–4.19	2.14–2.59	2.85–3.2
Subgenital plate length mm	2.3–3.0		2.2–3.0	
Subgenital plate degree	46.3–58.3		30.7–35.8	
3D measurements of the eyes				
Longitudinal height µm			482.72–709.17	458.61–760.13
Cross-sectional height µm	532.59–657.29	598.04–646.17	460.35–577.58	422.86–696.96
Length µm	2254.37–2462.66	2500.83–2737.3	1943.74–2137.79	2131.68–2469.35
Width µm	1321.6–1454.8	1412.78–1524.26	1055.54–1213.7	1162.68–1344.2
Volume μm^3	1071906358.87–1812003789.7	1566466980.82–1798593679.03	587729028.76–865630822.96	894156739.30–1428871850.17
upper valve degree		146–163		134–140
upper valve distance µm		165–240		115–208
upper valve width µm		160–311		106–180
degree of protrusion		106–135		57–100
protrusion line 1 µm		171–235		118–158
protrusion line 2 µm		104–137		86–118
protrusion distance µm		236–327		174–199
protrusion vertical distance µm		161.57–180.92		126.31–154.28

Etymology. The specific epithet is a Latin noun, meaning mouse. It refers to the species' very slender and delicate habitus.

Definition. The described species is assigned to the genus *Betiscoides* Sjöstedt, 1924 due to phylogenetic and overall morphological characteristics. The very slender, elongate, stick-like and medium sized body defines the species. The antennae are ensiform and triangular in cross-section. The head is acutely conical elongated and the end of the abdomen shows dense and long hairs. The arolium is large. The subgenital plate is elongate and acutely conical; the ovipositor is short with well-curved valves and sharp tips.

Diagnosis. This new species differs morphologically from the described ones mostly by its overall delicate habitus, the comparatively densly and longhaired end of the abdomen of the males. The body is smaller and more delicate than *Betiscoides meridionalis*. The head is more elongate than in *B. nova* and *B. parva*. The genital valves are strongly acute, sharply pointed, upper valve width narrower than in *Betiscoides meridionalis*. Just as *B. nova*, the new species represents a divergent evolutionary lineage as stated in Matenaar et al. (2018) being most closely related to *B. parva* (p-distance: 0.0734). As Key (1937) stated for *B. parva* and *B. sjostedti*, also this species is far less elongate than *Betiscoides meridionalis*, and *B. parva*, *B. nova* and *B. sjostedti* as well as *B. muris* are morphologically more similar to each other than any of these to *B. meridionalis*. Morphologically *B. muris* relates the most to *B. sjostedti* although *B. sjostedti* lacks the hairy end of the abdomen, which instead can be found even stronger in *B. parva* (Fig. 15). The genetic distance of *B. muris* to *B. meridionalis* is closer than to *B. nova* or *B. sjostedti*. The frontal ridge of the new species is more prominent and protruding than in *B. nova*; Fig. 16.

Description of the holotype. Body of medium length, slender, delicate (Figs 9B, 10B). BL 22.5 mm. Integument finely rugose, shiny golden. Antennae 22-jointed, ~ 6 mm, finely ensiform, slightly flattened above and slightly tapering, finely pointed and shiny, evenly punctured, in length longer than the head, reaching the pronotum. Left antenna between the 12th and 13th and on the 15th segment marked with shiny orange fluid-like spot. Head elongate, conical, from above almost 4 times as long as its width at the occiput and twice the diagonal length than the height, HL 3.8 mm, HDL 5.52 mm, HH 2.59 mm. Fv 1.4 mm, 0.7 the length of an eye, angular, the margins well raised but obtuse-angled, narrowing from the anterior margin of the eye forwards; callus line above the eyes culminating into the margins of Fv, (straight), strongly protruding in front of the eyes; median carinula faintly discernible on the fastigium. Head in profile convex above, face slightly incurved; angle acute (app. 49.4°). Apex of fastigium in profile slightly raised culminating dot-like at the very apex; frons oblique. Fr between the antennae in profile somewhat projecting, thin, lamelliform, lateral carinae distinct, below the antennae very narrow, shallowly sulcate, crossing the sulcus and only close to the clepeus at the basal part obliterated. Fc straight, distinct throughout. Eyes oval, 1 ¾ as long as their maximum width, their surface strongly convex, both margins somewhat curved, the upper more so than the lower, upper and lower margin slightly raised, as of callus. Ratio of eye length to fastigium length 0.61. PL 2.6 mm, lateral ventral length 1.78 mm, pronotum cylindrical, with weak median and indistinct lateral carinae; no sulcus crossing dorsum. Hind margin of metazona very slightly concave, anterior margin straight; sides of pronotum with the lower margin straight, anterior lower angle slightly more than 90°, rounded; posterior lower angle 90°, rounded. Pp destroyed through pinning. Mesosternal interspace reduced with mesosternal lobes connected. Anterior and middle legs strongly shortened. Tibia and tarsi haired, tarsi with black claws. Hind legs reaching beyond the end of abdomen. HFL 8.1 mm, hind femora very slender, about 5.5 times as long as their maximum width; outer apex of knees acute; hind tibiae with 10 outer and 13 inner spines. External apical spine of hind tibia present. Hind tarsus shorter than half of the length of the tibia. Arolium extremely large, its margin of beige color. Male supra-anal plate elongate, acutely angular. Cerci short, conical. Subgenital plate strongly elongate, 2.85 mm, acutely conical, 35.8°. End of abdomen with dense but fine, comparatively long hairs, see Fig. 15A. Supra-anal plate with the basal part about 0.65 the length of the apical part, the longitudinal depression distinct; the apical part of the plate shaped like an equilateral triangle with the base curved and the sides straight; apical angle widely rounded; no depression on the apical angle. Subgenital plate about twice the length of the supra-anal plate; comparatively sharply pointed; lower margin convex, upper margin straight; apex acute. Genital apparatus about 3.5 the length of one tergit. SGP: 2.85 mm, last three tergits: 2.32 mm ratio: 1.22. The total body volume is 5.38305e-08 m^3. The volume of the visible part of the eye is 587729028.76 μm^3. The longitudinal height being 493.28 µm, and the length 2137.79 µm. The cross-sectional height is 483.82 µm and the width itself is 1213.70 µm. General coloration dark-brown. Antennae, fore and middle legs and knees are slightly paler than the brown primary color of the body. The upper part of the head, thorax and abdomen, within the callus line, is beige. The Fv is dark brown almost black. A longitudinal stripe extends from the front of the head backwards along the central ridge of the body. The lateral stripe backwards from the base of the eye is beige-pink. It starts at the lower hind corner of the eye (as a somewhat raised callus ridge) and reaches the end of the middle leg. Eyes brown, hind femora of brown color processing into yellow beneath, knees, upper and lower external carina of the hind femur yellow. Hind tibia orange and brown in the lower side, spines and spurs black-tipped.

Description of the allotype. Larger than the male (Fig. 16I). BL 26.5 mm, antennae 22-jointed, ~ 5 mm. fastigium about as long as an eye. The anterior and posterior margin of the eye are somewhat raised, as of torus. HL

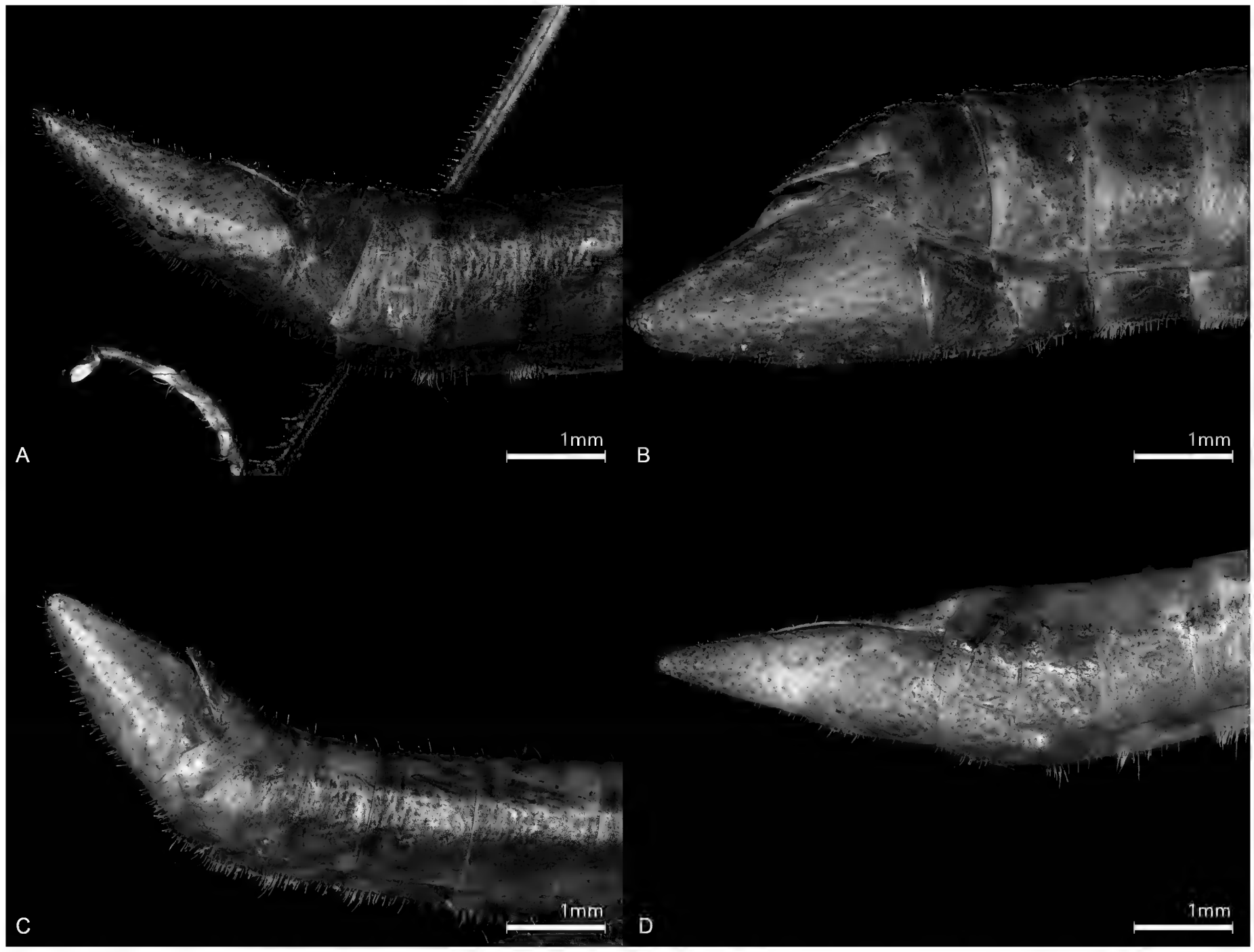

Figure 15. Images of the end of the abdomen of specimens **A.** HLMD-Cael-364HT, B156 (*Betiscoides. muris* sp. nov.); **B.** HLMD-Cael-4HT, B168 (*B. nova* sp. nov.); **C.** *B. parva* (HLMD-Cael-381, B103) and **D.** *B. sjostedti* (HLMD-Cael-382, B21).

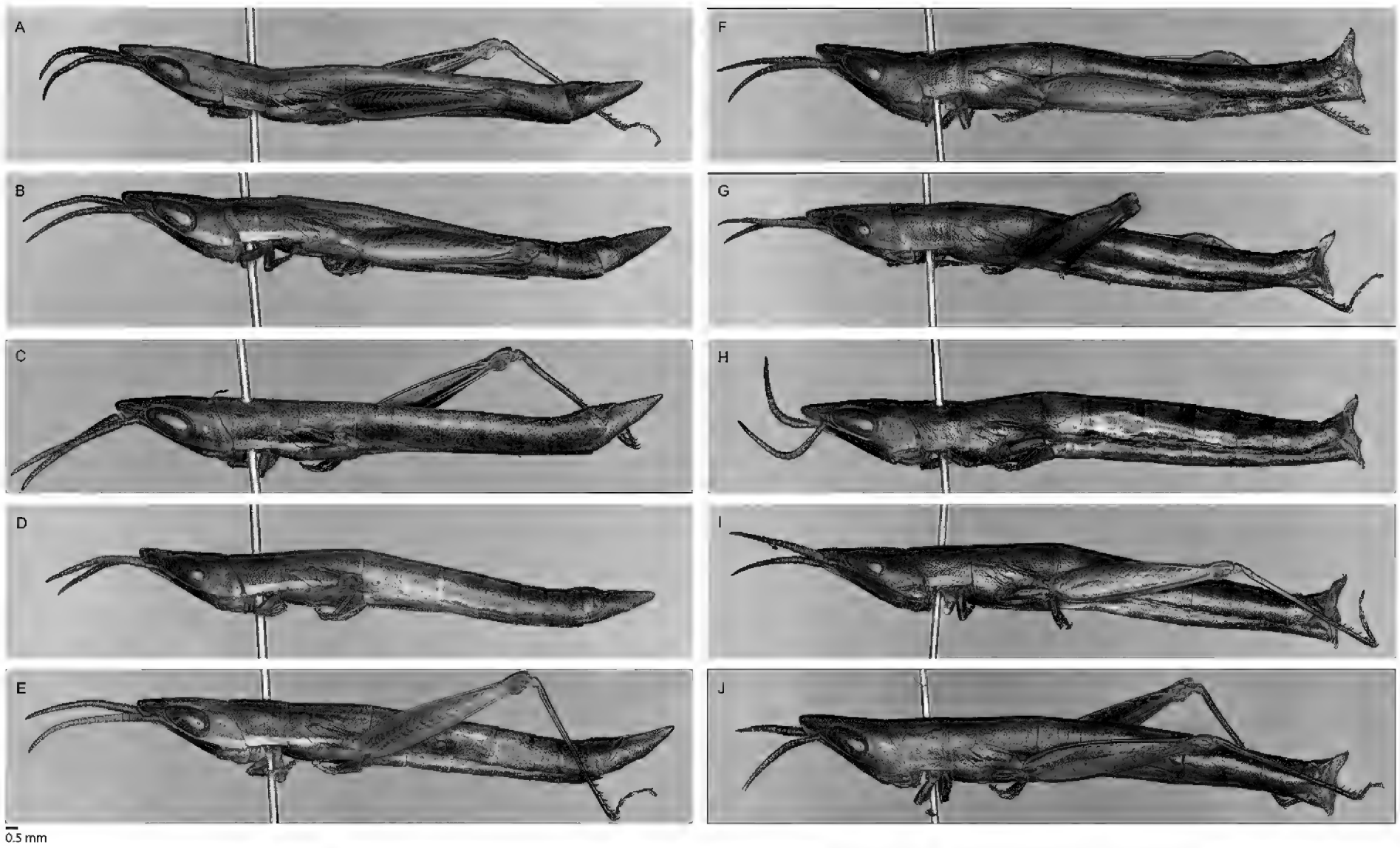

Figure 16. Lateral views of female and male type specimens *B. muris* sp. nov. **A–D.** HLMD-Cael-360-363PT; **E.** HLMD-Cael-364HT, B156; **F–H.** HLMD-Cael-365-367PT; **I.** HLMD-Cael-368AT, B155; **J.** HLMD-Cael-369PT.

4.3 mm, HDL 5.89 mm, HH 2.92, head in profile acute-angled (50.9°). PL 3 mm, sides of pronotum with lower margin straight; anterior margin sloping forward, only very slightly incurved, posterior margin very little incurved, sloping forward in the upper part. Anterior lower angle more than 90°, posterior lower angle 90°, both rounded. Pp T-shape, proximal concave, 673.43 µm in length, anterior part 233.54 µm width and 52.87 µm higher than the posterior part (of 122.29 µm width, see Figs 17, 18), fine and thin hairs on the broader anterior part and at the sides only. HFL 9 mm, hind tibiae with 10 outer spines, 11 inner spines. Protrusion of lower genital valves crossed by two diagonal sulci. Pr lines 1 and 2 slightly curved, bending inwards, apex of Pr thereby rounded although degree of protrusion strongly acute (79°), Pr line 1 slightly longer (155 µm) than Pr line 2 (91 µm), Pr distance is 199 µm, Pr area is of 12455.69 µm^2 and protrusion vertical distance is 129.66 µm, protrusion to tip of valve distance (horizontal distance) is 330.13 µm (see Fig. 13B). Tips of the valves black and strongly acute. End of upper valve slender and acute pointed, of 134°, upper valve distance 173 µm, upper valve width is 173 µm. General coloration similar to, but slightly less dark, than that of the male. Eyes and hind femora, both outside and inside, paler than the rest of the body; outer side of femur with black stripe and fishbone pattern; hind tibiae darker than the femur but without gradient in color. The volume of the visible part of the eye is 1356324476.51 µm^3. With longitudinal height being 760.13 µm, and the length 2131.68 µm. The cross-sectional height is 696.96 µm and the width itself is 1175.43 µm.

Variation. The antennae are 22–23-jointed and the segments are covered with fine, black dots and shiny appearance in all specimens. Posterior margins of the antennae segments of one male specimen are matt beige, while the rest is of the usual common shiny brown color. Specimens show little differences in the shape of the head in profile, varying from described morphology of the holotype to a slightly more concave form. Similar to *B. nova*, the face varies concerning the degree of distinction of the lateral carinae below the sulcus and the shape of the sulcus itself. In some specimens, the lateral carinae are distinct throughout, also beneath the sulcus. The sulcus is shaped as a mustache sometimes. This intraspecific variation is not sex-specific. Variation in spines on the hind tibia: In male, the hind tibiae had 9–10 outer and 10–14 (!) inner spines. In females, the hind tibia showed 9–10 outer spines and 11–13 inner spines. In contrast to the other known species of *Betiscoides*, there seems to be a intraspecific variability

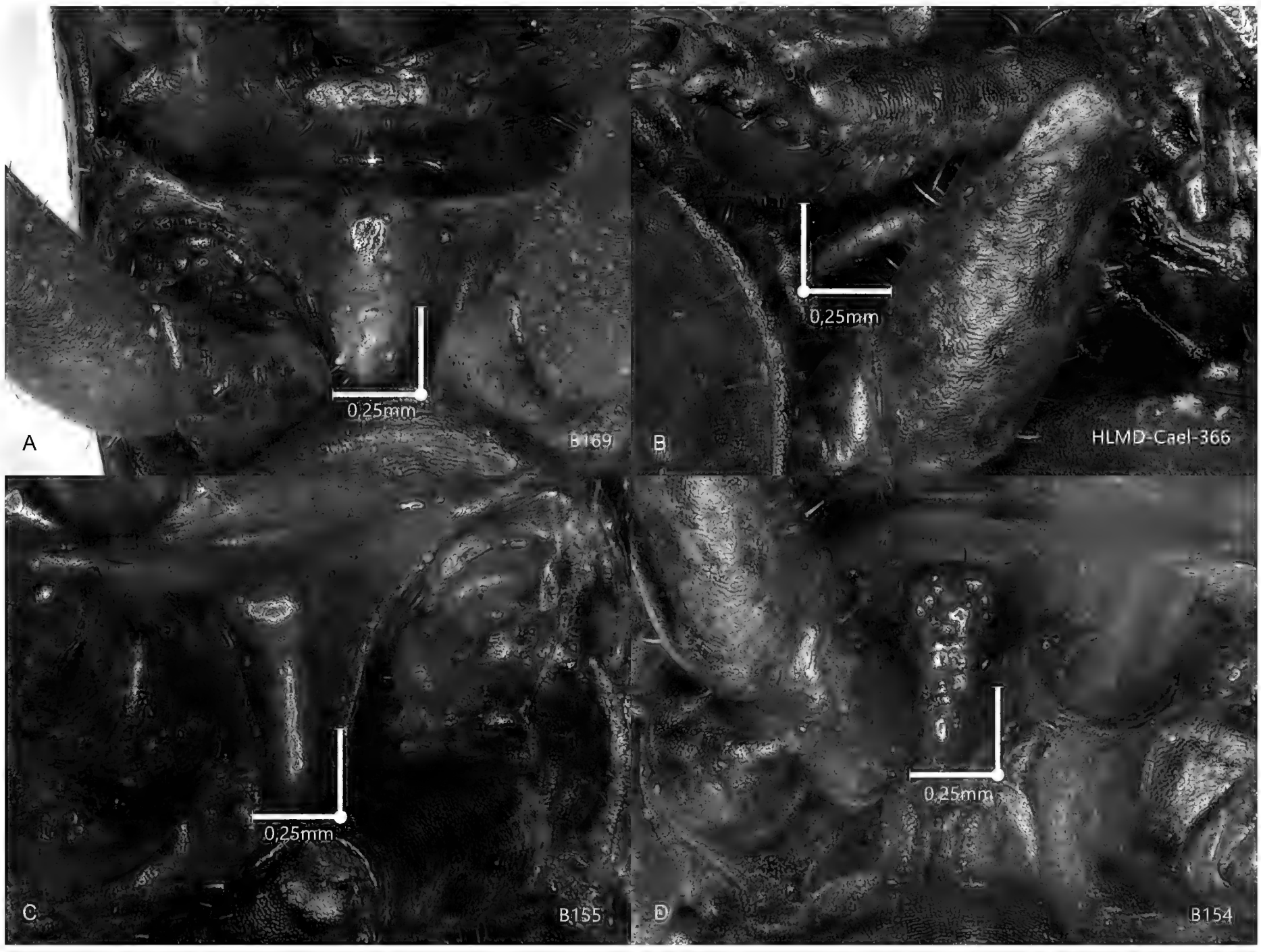

Figure 17. High resolution DOF images of the prosternal process of *Betiscoides muris* sp. nov. clustering in DEL 22, Groot Winterhoek, revealing four different shapes of Pp. **A.** Image of HLMD-Cael-379PT, B169; **B.** Image of HLMD-Cael-366PT; **C.** Image of allotpye HLMD-Cael-368AT, B155; **D.** Image of HLMD-Cael-367PT, B154.

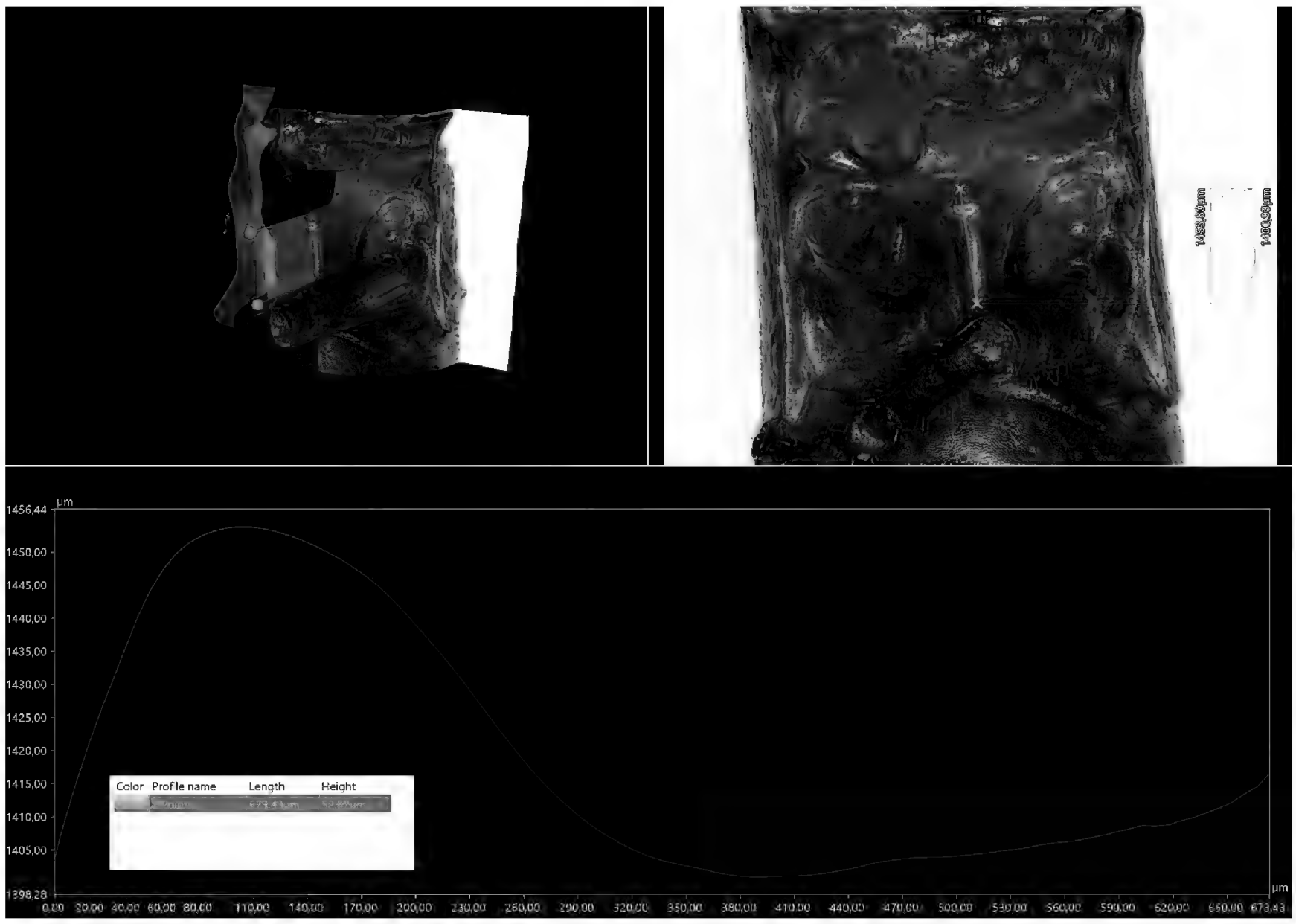

Figure 18. 3D-image of the prosternal process of the allotype of *Betiscoides muris* sp. nov. HLMD-Cael-368AT, B155. The output of the 3D profile image analysis is shown, including the curve progression from the anterior to the posterior part in profile, and total length and height.

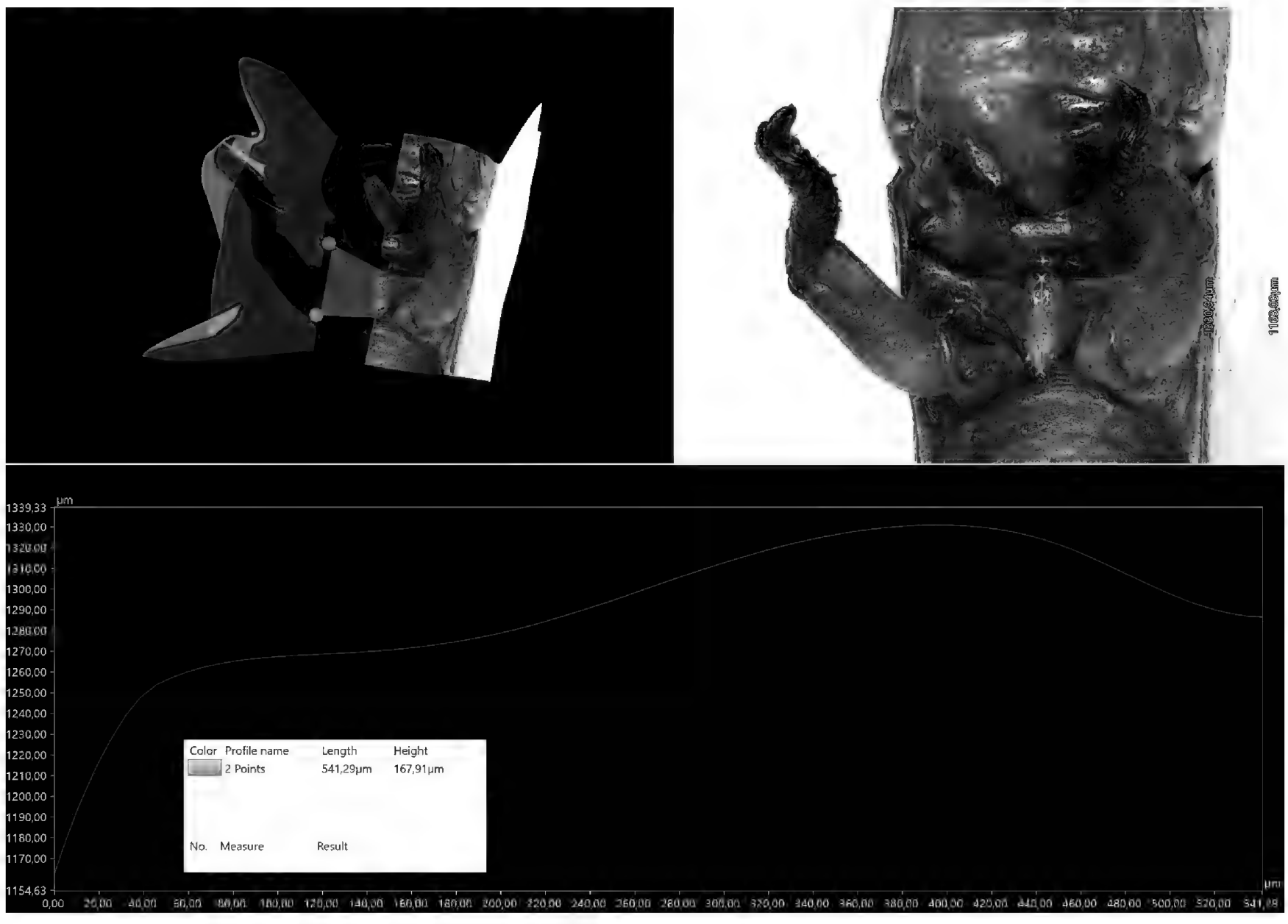

Figure 19. 3D image of the prosternal process of *B. muris* sp. nov. specimen HLMD-Cael-379 PT, B169. The output of the 3D profile image analysis is shown, including the curve progression from the anterior to the posterior part in profile, and total length and height.

in the shape of the prosternal process, in general the Pp is about twice as long as broad, its margins and angles rounded; the anterior end little broader than the posterior. However, four different shapes can be distinguished within the *B. muris* species, making the Pp itself a variable character within this species (see Fig. 17): a) thin lamelliform (one thin line from above), b) trapezoid, c) T-Shape, d) thick lamelliform. Furthermore, the trapezoid and thick lamelliform Pps are often tuberculate and hairy, whereas T-shape and thin lamelliform ones are rather smooth and not very rugose. The 3D image analysis revealed variations in the elevation of the prosternal process. In some specimens, the anterior part is higher than the posterior and vice versa (see Figs 18,19). The Pp of specimen HLMD-Cael-379PT, B169 is 541 µm long and the posterior part is 167.91 µm higher than the anterior; the Pp of specimen HLMD-Cael-367PT, B154 is 614.53 µm long and the posterior part is 148.39 µm higher than the anterior. General coloration in males dark-brown. Antennae, fore and middle legs are of the same brown primary color as the body. The upper part of the head, thorax and abdomen, within the callus line, is of light brown, orange or yellow color. The lateral stripe backwards from the base of the eye is beige. It starts at the lower hind corner of the eye (as a somewhat raised callus ridge) and stops right behind the middle leg. In one male, the stripe seems to extend to the femur as a yellow line. Eyes brown, hind femora pale, especially when light brown within the callus line, or with blueish line. In life, sometimes of green color (Fig. 20). Knees light brown. Hind tibiae brown, spines and spurs black-tipped. Female: General primary coloration similar to that of the male. No variation toward green or light brown color within the callus line. Hind femora, both outside and inside, paler than the rest of the body, varying in one female towards blue, femoral stripe often present, herring bone pattern distinct hind tibiae brown. Detailed measurements are provided in Table 1.

Specimen HLMD-Cael-379PT, B169 is not included in the subgenital plate degree measurement due to damage.

Figure 20. Male individual of *Betiscoides muris* sp. nov. from Groot Winterhoek Wilderness Area, South Africa in life; image taken on 06 March 2020, 32°58'54.76"S, 19°3'18.37"E.

Distribution, ecology and conservation status. Described from six males and five females from Groot Winterhoek, Western Cape, South Africa, collected in 2016 and 2020. The species occurs on the plateau of the Groot Winterhoek Nature reserve in restio-dominated wetland. It is abundant in patches with water covering the bare ground between the single restio plants. As the three formally recognized species of *Betiscoides* are considered "endangered" (Hochkirch 2012a, 2012b, 2012c), I propose this status as well for *B. muris* as this species is only known to occur at a single locality and its habitat is in decline.

Key to species

1 Body elongate, head in profile conical, fastigium of vertex shorter than twice the length of eye 2
– Body very elongate, head in profile acutely conical, fastigium of vertex nearly twice the length of eye ..... *B. meridionalis*
2 Body smooth..... 3
– Body finely but densely haired..... 4
3 Body slender, head conical, eyes ovate, male subgenital plate comparatively short, apex pointed in profile..... *B. sjostedti*
– Body robust, head in profile as long as high, eyes large and ovate, male subgenital plate elongate, apex rounded in profile ..... *B. nova*
4 Body short, head conical but less elongate, eyes ovate and very prominent, tarsus half the length of the hind tibia..... *B. parva*
– Body of medium length, head conical and elongate, its diagonal length twice its height, eyes ovate but not protruding, tarsus shorter than half the length of the tibia ..... *B. muris*

An overview of the main morphological differences between the species is provided in Table 2.

Table 2. Description of the shape of the morphological characters with the main differences of the five *Betiscoides* species.

Morphological character	*B. meridionalis*	*B. parva*	*B. sjostedti*	*B. nova* sp. nov.	*B. muris* sp. nov.
Body	very elongate, very slender	slender, short	slender, medium length	robust, medium to large	delicate, slender medium length
Head	acutely conical, very elongate	conical, less elongate	conical, elongate	conical, in profile as long as high	conical, very elongate
Eyes	ovate, flat	ovate, large prominent	ovate	ovate, large, less prominent than in *B. parva*	ovate, not protruding
Prosternal process	strongly lamelliform, compressed	slightly lamelliform, anterior end broader and higher	slightly lamelliform, anterior end a little broader	trapezoid, flat, two kinds of hairs	very variable, one kind of hair
Subgenital plate	extremely elongate and acutely pointed	elongate, hairy, apex rounded	comparatively short, smooth, pointed	elongate, smooth, in profile: apex rounded	very elongate and acutely pointed, hairy
Female ovipositor valves	recurved, apex acute, Pr apex acute	short, recurved, apex rounded	long, recurved, apex acute	recurved, apex rounded, Pr and Pr apex rounded	recurved, apex and protrusion strongly acute, Pr apex rounded

Discussion

Revealing morphological traits among cryptic species or divergent evolutionary lineages is a challenging but important task to firstly, obtain an overview of the global biodiversity and its distribution and secondly, to provide for the basis of species conservation actions. The application of deep learning and image based identification tools increased strongly in the last decade (Amarathunga et al. 2021) and seems indispensable. The presented results revealed that fine scale morphological analysis is a promising approach for taxonomic assessments, which will eventually influence the further development of deep learning algorithms as well. I will discuss some of the findings in more detail.

Achieved morphological results

Head

The ratio of the eye length to the fastigium length were diagnostic characters used for discriminating *B. meridionalis*, *B. parva* and *B. sjostedti* and was provided in addition to the description by Key (1937). However, the respective ratios turned out to be rather similar in *B. nova* and *B. muris* (0.60 and 0.61), and thus, are not diagnostic for these two species. The diagonal and dorsal length of the head as well as its height, i.e. the respective ratios, turned out to be diagnostic characters, which were used in the key. Little intraspecific variability was found among females of *B. muris* in terms of the diagonal head length, only one specimen exhibited an exceptional greater HDL (6.62 mm versus around 5.87 mm in all other females).

Hair – quantitative analysis

The DELs of *Betiscoides* differ, inter alia, by the amount of hairs at the end of the male abdomen. In this study, I was able to show that *B. parva* is overall very hairy which led to the redefinition of the genus characteristics. Differences in this character state are particularly evident in sympatrically distributed lineages. For instance, DEL 11 and DEL 16 that occur sympatrically in Limietberg/ Du Toitskloof, show differences in the amount and length of the hairs at the end of the abdomen (see Fig. 21). Image analysis worked well on the clearly haired specimens but it did not work properly on sparsely haired specimens. For the moment, it would be sufficient to gain approximate data on the amount of hairs to achieve sufficient detection in differences and to distinguish the DELs when combining this trait with other diagnostic characters. Although highly divergent genetically, the DELs 11 and 16 were not described and named as new species as the number of available voucher specimens is too low to allow for their sufficient external morphological description. In *B. meridionalis*, hairiness might likely turn out to be a diagnostic character as well, however hairiness in that species can be considered low and was very variable among the specimens of DEL 3. Thus, I refrained from revising that character and followed the description by Key (1937). A fully automated analysis is not possible for now. In order to count the hairs by framing the abdomen, only few steps are required and the image analysis itself works fast. However, the assessment of the total number of hairs is hampered by the insufficient detection of hairy structures, as they cannot be separated from other bright structures on the body and thus, cannot be counted automatically. Nevertheless, hairs or the hairiness of specimens have always been important diagnostic characters in species delimitation of Orthoptera (Dirsh 1965) and high resolution imagery brings the analytical diagnosis to a new level, adding diagnostic features that are of course missing or erroneously described in the historical literature, as is here the case with Key (1937).

Female genital characters

Detailed measurements of the external genital characters of the females resulted in consideration of additional character states, which can be used to distinguish among species. There was no overlap between the measured values except for “upper valve width” and “protrusion line

2". However, the combination of the female genital characters serves as a solid base to distinguish between the species. "Vertical distance of protrusion" was also an efficient measure to distinguish between the species, despite some intraspecific variations. However, images need to be of very good quality and need to be controlled prior the subsequent image analysis. Specimen HLMD-Cael-12PT either showed high variability or was in a different state of decay, either way; the protrusion itself is folded towards the body center, which could only be recognized in 3D mode. Thus, measuring from the tip of the protrusion to the tip of the valve resulted in a lesser vertical distance. In such cases, I advise to set the point on the tip of protrusion at a slightly higher point to ensure the actual level of the protrusion is met.

Profile analysis of prosternal process

The integrative taxonomic approach revealed that the Pp is a plastic character within *B. muris*, which can be classified in four different states some of which are described for *Betiscoides* for the first time. Results of the phylogenetic reconstruction made clear that these states are not diagnostic to delimitate species. The 3D analysis of the specimens' Pps revealed that the first impression of a proximal concave Pp turned out to be false. Only by turning to the side of the process and the profile analysis, it became clear that the surface was not sunken in at all but there is a slight gradient towards the posterior end of the Pp. This procedure worked also for even finer structures and lines, which seemed to be small sulci in 2D view but were in fact not existent when analyzed in profile. Unfortunately, in order to conduct the profile analysis the Pp needs to be recorded in straight top ventral view as different angles falsify the results. However, sufficient Pps could be analyzed and revealed no variation regarding the curve progression of the Pps in *B. nova* and could precisely show that this diagnostic character is highly variable in *B. muris*. The gradient of the Pp towards either the anterior or posterior edge is a diagnostic character for *B. parva* and *B. sjostedti* (Key 1937) and the shape is diagnostic for *B. nova* but not for *B. muris*. In addition, the simple measurement of the anterior and posterior width was much more accurate using the extended depth of field images than measuring by measuring eyepiece. Depth compositing image revealed that *B. nova* features two kinds of hairs on its Pp and it requires further research to assess their function.

Volume – Body and eyes

Using fully calibrated and referenced EDOF based 3D models of insects is rather novel in species descriptions (Hoenle et al. 2020) and this is the first time, the derived body volume is presented and included in a species description. The analyzed specimens were collected and preserved in the same manner and under the same conditions, allowing for the comparisons and providing a quantitative support of the qualitative perception (order: *B. nova* > *B. meridionalis* > *B. sjostedti* > *B.muris* > *B.parva*). In general, the state of preservation always affects morphometric analyses and specimen HLMD-Cael-379PT, B169, which had been dried after killing and wetted again before pinning, had been flattened at its abdomen as result of this preparation process. It is of course obvious that the specimen's state influences results of 3D measurements. Specimens of *B. muris* were preserved quite well when kept frozen until pinning. Thus, it is of advantage to measure specimens as soon as possible after collection, especially for specimens of dry collections. However, the effect of dried preservation differs within Orthoptera and among taxa. For instance, Coleoptera are less prone to external decay due to the very robust integument are more robust than Orthoptera. Specimens that are preserved in ethanol are subject to total body volume loss, but when stored in the right concentration, eye measurements will benefit from this method of preservation and it therefore is to be favored over dry preparation. In order to avoid deflection of the body over time, it can be helpful to store specimens in fitting vials. Deflection causes inaccurate results in 1D or 2D measurements but can be neglected when applying 3D volume measurements of the specimens' bodies. Disadvantage of pinning turned out to be significant regarding the preservation of the prosternal process, which is easily destroyed by the needle. This is often prevented if an expert pins the specimens, but that is unfortunately often not the case, even in museum collections.

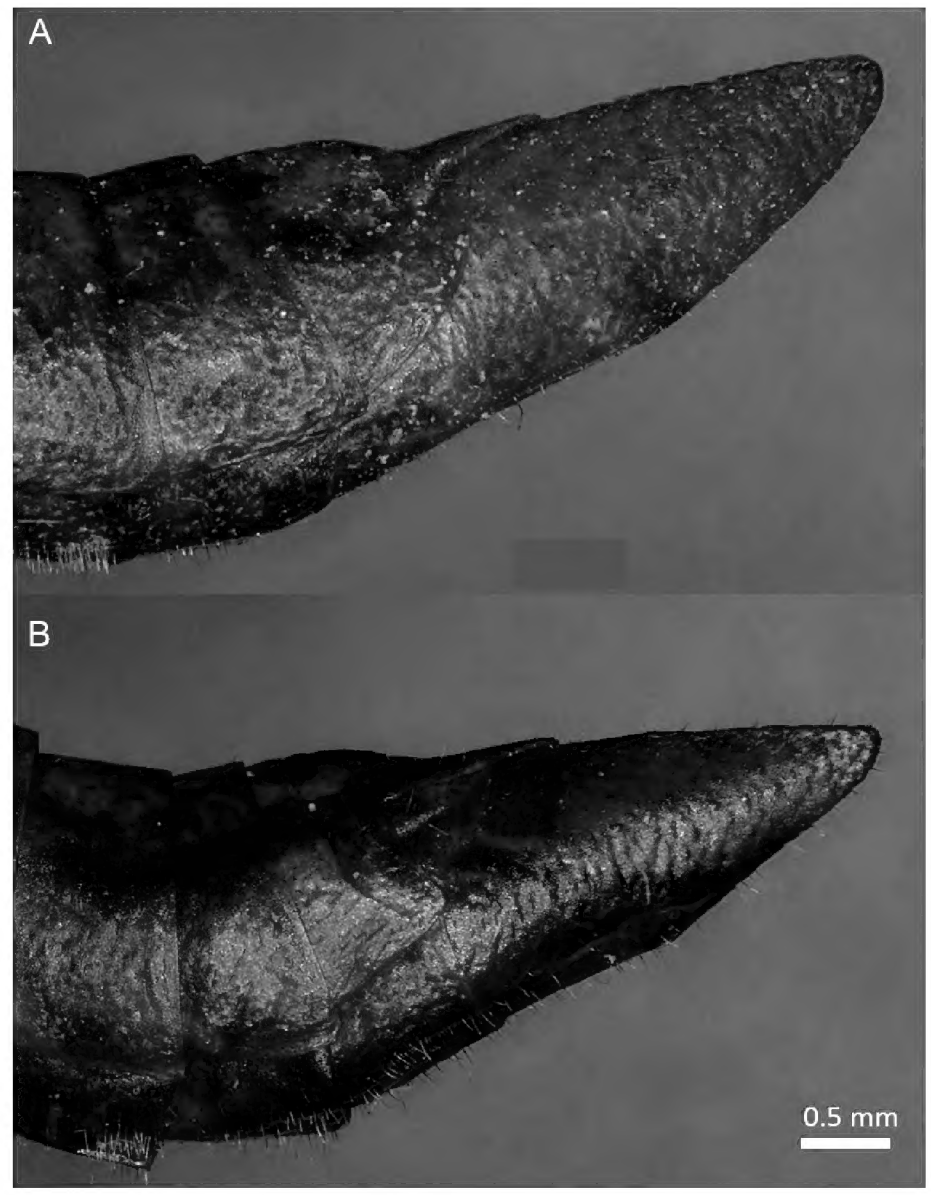

Figure 21. End of abdomen of *Betiscoides* sp. specimens B134 from DEL 16 (**A**) and B128 from DEL 11 (**B**), collected at Limietberg, Du Toitskloof, study site 34.

3D measurement of the eyes revealed that the eyes' volume is sexually dimorphic within *B. muris* but not in *B. nova*. It remains challenging to calculate the volume and other 3D eye characters because of the degree in decay of dried specimens. However, the advantage is that it is easy to evaluate the specimens' state and to decide to not consider it if conditions appear inappropriate. Species like *Betiscoides*, which feature very prominent eyes and are regarded as morphologically cryptic, benefit from integrating this new evaluation of character states into future descriptions as they possibly very often will turn out to be diagnostic. In eyes of *B. muris*, the longitudinal height correlated negatively with length, meaning the shorter the eye was, the higher was the longitudinal height. Regarding the body volume, it interesting for species like *Betiscoide*s sp. to compare the body volume with the equivalent piece of blade of the respective host restio plant to look for a certain morphological adaptation or mimicry.

Taxonomy of *Betiscoides*

The 3D measurement approach applied provided evidence for the existence of morphological differences between the cryptic divergent evolutionary lineages of *Betiscoides* and further collecting and analyses is needed to resolve the taxonomy of this highly diverse group. The integrative taxonomic approach allows to conclude that all DELs can be assigned to the genus *Betiscoides*, due to the the phylogeny and overall morphology.

Future relevance of integrating 3D measurements as taxonomic tools

The application of standardized, calibrated and high-resolution digitization is a novel technique to enable the detection of fine scale morphological differences, which requires access to specific equipment and technology. At first, this seems to be a barrier to achieve an effective and repetitive procedure in taxonomic work. However, on the long term exactly these procedures shall enable an even more rapid identification as deep learning [AI] tools become more common. Applying 3D image technology enables you to describe what you actually see and to put this into numbers and objective relations. You can measure what you really see, or you can finally see how it really is! Furthermore, this is a noninvasive approach, which does not damage or even destroy the specimens and might even work on living individuals in the field. Thus, it is a worthwhile investment to achieve simpler, comparable and reliable identification in the future.

Similar to other digital morphometric analyses and attached imaging techniques, one advantage in photogrammetry is that measurements are often very exact since the high resolution makes it easy to set measuring points accurate and, if measuring lines are inserted in the image, the methods of measuring a certain distance remains traceable. Especially on dried and pinned material, photogrammetric methods are often the more suitable ones compared to micro-tomography as the needle likely causes artifacts in the latter and inner organic structures have often decomposed anyway (Ströbel et al. 2018). Thus, it is also very useful to apply this method on old type material to allow precise taxonomic analyses and reveal external morphological differences, as there is often no information on inner genitalia available in the species' descriptions. This is also the case in *Betiscoides*.

As important as imaging analysis and deep learning are, it still requires (human) taxonomic expertise to avoid misinterpretation of plastic characters, especially in almost cryptic species, or physical changes during life span. As also suggested before (Høye et al. 2021), integrating sufficient molecular, and fine scale morphological character information into deep learning algorithms should effectively support correct assessment and assignment in the future. In order to achieve this goal, it is necessary to train deep learning algorithms properly (Amarathunga et al. 2021; Høye et al. 2021) and to optimize mobile devise camera optics. When applicable, bioacoustics are also integrated into deep learning algorithms (Høye et al. 2021) and information of other types of communicational behavior should be fed into deep learning algorithms to include this valuable information.

Deriving standards for sustainable application of photogrammetric taxonomic identification

In order to gain robust und replicable photogrammetric measurements, certain standards should be considered. If applicable, the specimen should be digitally processed as soon as possible after killing/ preparation. This avoids misleading measurements due to decay, which of course is especially important if referring to fine scale traits. Specimens should be prepared or dissected as carefully as possible to conserve possible diagnostic characters and assure that these remain visible. When taking the images bound for volume and further 3D measurements, magnification to full screen or stitching is necessary to achieve reproducible results. Images should be taken in top view, meaning the image degree should be 0° and the specimen should be placed in dorsal, ventral, or lateral position; and checked for the point height prior to further analysis to gain replicable and reliable results. When conducting 2D plane measurements, I advise to zoom into or very close to the area where the point marks will be set and to describe in detail where the ruler was placed.

Data deposit

The sequences reported in this paper have been deposited in the Genbank database (accession nos. MG243722-

MG244189; accession nos. listed in Matenaar et al. (2016); accession nos. PP411595–PP411603, PP417657–PP417676). For additional information, see Suppl. material 1.

Acknowledgments

I wish to thank SANParks, CapeNature, and Eastern Cape Park and Tourism Agency for providing the permits and for their continuous support over the last 13 years. I thank Trier University and Stuttgart Statemuseum of Natural History for their financial support during the respective collecting trips. I also thank Nico Blüthgen and Chris von Beeren for providing access to the molecular lab of Ecological networks (TU Darmstadt). Special thanks to Antonia Späth for building the 3D models and to Jörn Köhler for the valuable comments on the manuscript. I would also like to thank the reviewers for their constructive feedback and time.

References

Amarathunga DC, Grundy J, Parry H, Dorin, A (2021) Methods of insect image capture and classification: A Systematic literature review. Smart Agricultural Technology 1: 100023. https://doi.org/10.1016/j.atech.2021.100023

Blaxter M, Mann J, Chapman T, Thomas F, Whitton C, Floyd R, Abebe E (2005) Defining operational taxonomic units using DNA barcode data. Philosophical transactions of the Royal Society of London. Series B, Biological sciences 360(1462): 1935–1943. https://doi.org/10.1098/rstb.2005.1725

Cigliano MM, Braun H, Eades DC, Otte D (2023) Orthoptera Species File - Lentulidae Dirsh, 1956. https://orthoptera.speciesfile.org/otus/822677/overview [accessed on 19.12.2023]

Dirsh VM (1965) The African Genera of Acridoidea. Cambridge, UK: Cambridge University Press.

European Commission [Directorate General for Environment] (2022) European Red List of insect taxonomists, Publications Office.

Green J, Holmes L, Andrew J, Westoby M, Oliver I, Briscoe D, Dangerfield M, Gillings M, Beattie AJ (2004) Spatial scaling of microbial eukaryote diversity. Nature 432(7018): 747–750. https://doi.org/10.1038/nature03034

Hawlitschek O, Morinière J, Lehmann GUC, Lehmann A W, Kropf M, Dunz A, Glaw F, Detcharoen M, Schmidt S, Hausmann A, Szucsich NU, Caetano-Wyler SA, Haszprunar G (2017) DNA barcoding of crickets, katydids and grasshoppers (Orthoptera) from Central Europe with focus on Austria, Germany and Switzerland. Molecular Ecology Resources 17(5):1037–1053. https://doi.org/10.1111/1755-0998.12638

Hochkirch Axel (2012a) Betiscoides meridionalis. IUCN Red List of Threatened Species. https://www.iucnredlist.org/species/17476731/17477270 [accessed on 14.12.2023]

Hochkirch A (2012b) Betiscoides parva. IUCN Red List of Threatened Species. https://www.iucnredlist.org/species/17476704/17476715 [accessed on 18.12.2023]

Hochkirch A (2012c) Betiscoides sjostedti. IUCN Red List of Threatened Species. https://www.iucnredlist.org/species/17477286/17477290 [accessed on 18.12.2023]

Hoenle P, Lattke JE, Donoso D, von Beeren C, Heethoff M, Schmelzle S, Argoti A, Camacho L, Ströbel B, Blüthgen N (2020) *Odontomachus davidsoni* sp. nov. (Hymenoptera, Formicidae), a new conspicuous trap-jaw ant from Ecuador. ZooKeys 948: 75–105. https://doi.org/10.3897/zookeys.948.48701

Høye TT, Ärje J, Bjerge K, Hansen OLP, Iosifidis A, Leese F, Mann HMR, Meissner K, Melvad C, Raitoharju J (2021) Deep learning and computer vision will transform entomology. Proceedings of the National Academy of Sciences of the United States of America 118(2): e2002545117. https://doi.org/10.1073/pnas.2002545117

Huelsenbeck JP, Ronquist F (2001) MRBAYES: Bayesian inference of phylogenetic trees. Bioinformatics 17(8): 754–755. https://doi.org/10.1093/bioinformatics/17.8.754

Key KHL (1937) New Acridiidae from South Africa. Annals of the South African Museum 32: 135–167.

Kumar S, Stecher G, Li M, Knyaz C, Tamura K (2018) MEGA X: Molecular Evolutionary Genetics Analysis across computing platforms. Molecular Biology and Evolution 35(6): 1547–1549. https://doi.org/10.1093/molbev/msy096

Lanfear R, Calcott B, Ho SYW, Guindon S (2012) Partitionfinder: combined selection of partitioning schemes and substitution models for phylogenetic analyses. Molecular Biology and Evolution 29(6): 1695–1701. https://doi.org/10.1093/molbev/mss020

Larsen BB, Miller EC, Rhodes MK, Wiens JJ (2017) Inordinate fondness multiplied and redistributed: the number of species on Earth and the new pie of life. The Quarterly Review of Biology 92(3): 229–265. https://doi.org/10.1086/693564

Li X, Wiens JJ (2023) Estimating Global Biodiversity: The Role of Cryptic Insect Species. Systematic Biology 72(2): 391–403. https://doi.org/10.1093/sysbio/syac069

Matenaar D, Bröder L, Hochkirch A (2016) A preliminary phylogeny of the South African Lentulidae. Hereditas 153(1): 1. https://doi.org/10.1186/s41065-015-0005-6

Matenaar D, Fingerle M, Heym E, Wirtz S, Hochkirch A (2018) Phylogeography of the endemic grasshopper genus *Betiscoides* (Lentulidae) in the South African Cape Floristic Region. Molecular Phylogenetics and Evolution 118: 318–329. https://doi.org/10.1016/j.ympev.2017.09.024

Mora C, Tittensor DP, Adl S, Simpson AGB, Worm B (2011): How many species are there on Earth and in the ocean? PLOS Biology 9(8): e1001127. https://doi.org/10.1371/journal.pbio.1001127

Otte D (2014a) Twenty-nine new species in the genus *Leatettix* (Acridoidea: Lentulidae) from the Southern, Western and Northern Cape, South Africa. Transactions of the American Entomological Society 140(1): 349–401. https://doi.org/10.3157/061.140.0101

Otte D (2014b) Twenty-six new species of grasshoppers from the southern african arid zone (Orthoptera: Acridoidea: Lentulidae). Transactions of the American Entomological Society 140(1): 293–347. https://doi.org/10.3157/061.140.0116

Otte D (2015) Revision of the genus *Eremidium* Karsch with descriptions of sixteen new species (Acridoidea: Lentulidae). Transactions of the American Entomological Society 141(3): 499–544. https://doi.org/10.3157/061.141.0310

Otte D (2020) Thirty-two new south african grasshopper species in the family Lentulidae belonging to eleven genera (Orthoptera: Acridoidea). Transactions of the American Entomological Society 146(1): 1. https://doi.org/10.3157/061.146.0101

Otte D, Cowper G, Armstrong A (2023) Revision of *Lentula*, *Nyassacris*, *Basutacris* and *Qachasia*, with descriptions of three new genera and 26 new species (Acridoidea: Lentulidae). Transactions of the American Entomological Society 149(2):185–234. https://doi.org/10.3157/061.149.0205

Poulin R, Pérez-Ponce de León G (2017) Global analysis reveals that cryptic diversity is linked with habitat but not mode of life. Journal of Evolutionary Biology 30(3): 641–649. https://doi.org/10.1111/jeb.13034

Rambaut A (2016) Figtree 1.4.3. http://tree.bio.ed.ac.uk/software/figtree/

Ronquist F, Huelsenbeck JP (2003) MrBayes 3: Bayesian phylogenetic inference under mixed models. Bioinformatics 19 (12):1572–1574. https://doi.org/10.1093/bioinformatics/btg180

Rosselló-Mora R, López-López A (2014) The Least Common Denominator: Species or Operational Taxonomic Units? In: Zengler K (Ed.) Accessing Uncultivated Microorganisms. From the Environment to Organisms and Genomes and Back. Hoboken: John Wiley & Sons, Inc, 117–130. https://doi.org/10.1128/9781555815509.ch7

Silvestro D, Michalak I (2012) raxmlGUI: a graphical front-end for RAxML. Organisms Diversity & Evolution 12(4): 335–337. https://doi.org/10.1007/s13127-011-0056-0

Sjöstedt Y (1924) [1923] West- und Südafrikanische Acridiodeen. Arkiv för Zoologi 15(22): 1–21 [1922–1924].

Stork NE (2018) How Many Species of Insects and Other Terrestrial Arthropods Are There on Earth? Annual review of entomology 63: 31–45. https://doi.org/10.1146/annurev-ento-020117-043348

Ströbel B, Schmelzle S, Blüthgen N, Heethoff M (2018) An automated device for the digitization and 3D modelling of insects, combining extended-depth-of-field and all-side multi-view imaging. ZooKeys 759(759): 1–27. https://doi.org/10.3897/zookeys.759.24584

Tolley KA, Bowie RCK, John MG, Price BW, Forest F (2014) The shifting landscape of genes since the Pliocene: terrestrial phylogeography in the Greater Cape Floristic Region. Fynbos: Oxford University Press, Oxford, 142–163. https://doi.org/10.1093/acprof:oso/9780199679584.003.0007

Supplementary material 1

Specimens collections sites and Genbank Acc. numbers

Author: Daniela Matenaar

Data type: pdf

Explanation note: Information on the collection locality (localitly, site no., coordinates) and Genbank Accession numbers of genes 12S rRNA, 16S rRNA + tRNA-Leu + NADH dehydrogenase subunit I (ND1) (NDS), NADH dehydrogenase subunit 5 (ND5), internal transcribed spacer 2 (ITS2) and Histone 3 (H3) of the sequenced *Betiscoides* specimens.

Link: https://doi.org/10.3897/evolsyst.8.117735.suppl1